Volume 44 Number 3 July 1988

PHILIPS TECHNICAL REVIEW

Etching III-V semiconductors

Bistability in quantum-well lasers

Chemical surface modification

Striations in a gas discharge

PHILIPS

Philips Technical Review (ISSN 0031-7926) is published by Philips Research Laboratories, Eindhoven, the Netherlands, and deals with the investigations, processes and products of the laboratories and other establishments that form part of or are associated with the Philips group of companies. In the articles the associated technical problems are treated along with their physical or chemical background. The Review covers a wide range of subjects, each article being intended not only for the specialist in the subject but also for the non-specialist reader with a general technical or scientific training.

The Review appears in English and Dutch editions; both are identical in contents. There are twelve numbers per volume, each of about 32 pages. An index is included with each volume and indexes covering ten volumes are published (the latest one was included in Volume 40, 1982).

Editors: Dr J. W. Broer
Dipl.-Phys. R. Dockhorn, Editor-in-chief
Dr E. Fischmann
Dr J. L. Sommerdijk
Ir N. A. M. Verhoeckx
Dr M. H. Vincken
Ir F. Zuurveen

Editorial assistants: H. A. M. Lempens
J. H. T. Verbaant

English edition: D. A. E. Roberts, B.Sc., M. Inst. P., M.I.T.I.

© N.V. Philips' Gloeilampenfabrieken, Eindhoven, the Netherlands, 1988.
Articles may be reproduced in whole or in part provided that the source 'Philips Technical Review' is mentioned in full; photographs and drawings for this purpose are available on request. The editors would appreciate a complimentary copy.

PHILIPS TECHNICAL REVIEW

Volume 44, No. 3, July 1988

Contents

Wet-chemical etching of III-V semiconductors 61
J. J. Kelly, J. E. A. M. van den Meerakker, P. H. L. Notten and R. P. Tijburg
Removing material by wet-chemical etching is an important process in the fabrication of III-V semiconductor components

Then and Now (1938-1988) 75

Bistability in quantum-well lasers 76
A. I. Kucharska, P. Blood and E. D. Fletcher
Special semiconductor-laser structures allow rapid switching between high and low light-output levels

Chemical modification of surfaces 81
J. J. Ponjeé and P. N. T. van Velzen
Surface modification — an effective new chemical technology

Striations in a gas discharge 89
F. C. van den Heuvel
The electrical circuit has an effect on optical instabilities in a gas discharge

Scientific publications 96

PHILIPS

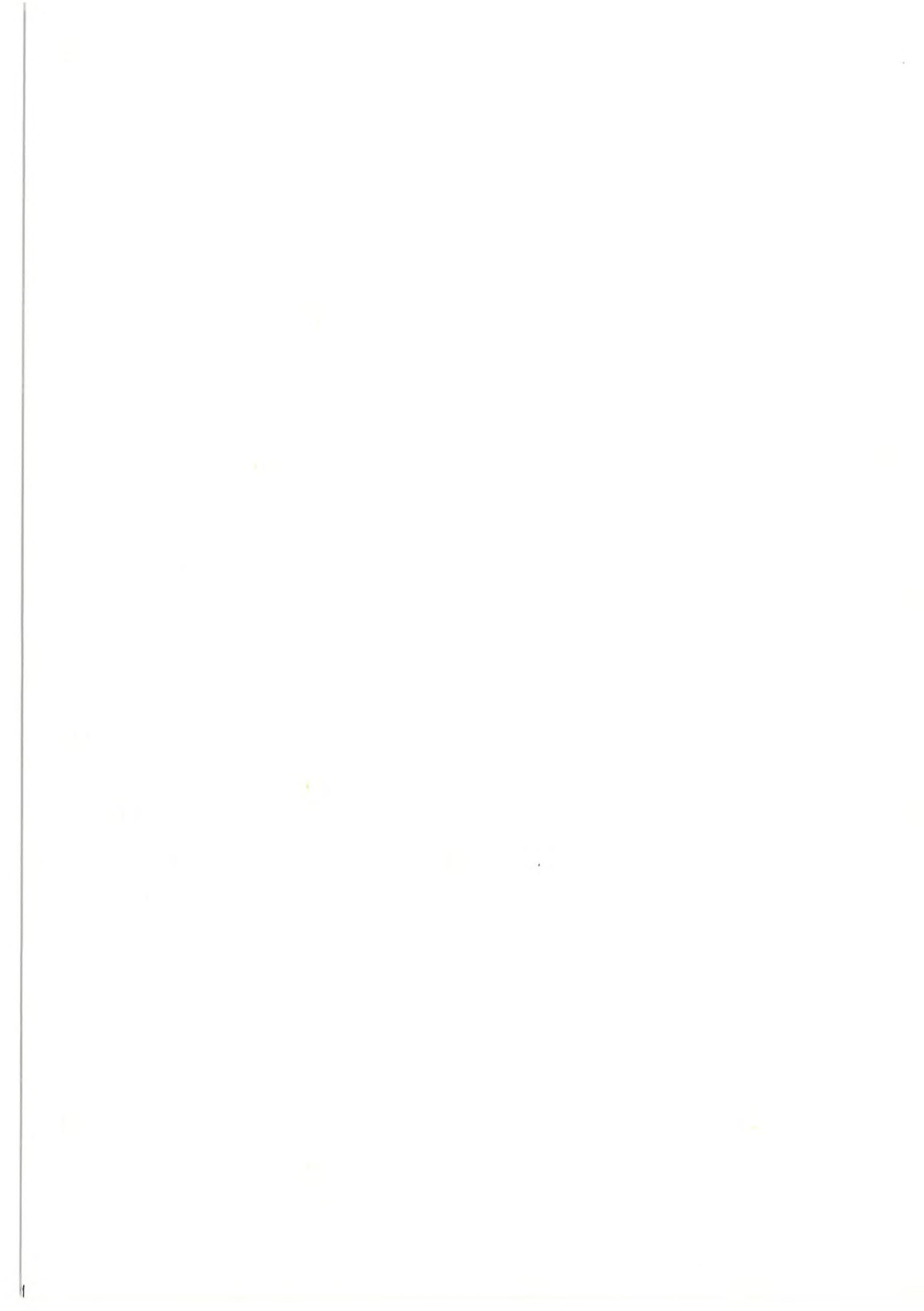

PHILIPS TECHNICAL REVIEW

Volume 44, No. 3, July 1988

Wet-chemical etching of III-V semiconductors

J. J. Kelly, J. E. A. M. van den Meerakker, P. H. L. Notten and R. P. Tijburg

In recent years the electronics industry has shown growing interest in semiconductors consisting of elements from groups III and V of the Periodic Table. This is largely because multilayer structures of such semiconductors have interesting applications. A well-known example is the semiconductor laser in the Compact Disc player, an important product for consumer electronics. Device structures with the required patterns can be obtained by dissolving parts of the semiconductor materials by a wet-chemical etching technique. Until recently wet etching was a relatively empirical process. An extensive study at Philips Research Laboratories in Eindhoven has provided a much better understanding of the etching behaviour of III-V semiconductors. One result is that the methods and etchants used in present applications can now be optimized more effectively and appropriate etchants can be developed for new applications.

Introduction

For many years the most widely used basic material in the semiconductor industry has been silicon. Since the seventies, however, we have seen the growing emergence of III-V semiconductors such as GaP, GaAs and InP for applications including light-emitting diodes, microwave field-effect transistors [1] and semiconductor lasers [2]. For these applications multilayer structures of different III-V semiconductors are used, which are grown epitaxially on a III-V substrate. A well-known combination is that of GaAs and $Al_xGa_{1-x}As$ in lasers with an emission wavelength of about 0.8 μm for Compact Disc players and digital optical recording [3]. Another well-known combination is that of InP and $In_xGa_{1-x}As_yP_{1-y}$ in lasers emitting at wavelengths of 1.30 and 1.55 μm for fibre-optic communications [4].

Multilayer structures are made with extremely accurate patterns to give them the required characteristics. Besides the mastery of the technique of producing different III-V semiconductors by epitaxial growth, this also requires an accurate etching technique for removing material at the right places. This is usually done by wet-chemical etching, although dry etching methods like plasma etching are occasionally used. III-V semiconductors can be etched to the required shapes by wet-chemical methods because the materials are generally perfect single crystals and the etch rate depends on the crystal orientation. The structure may often consist of a combination of materials

Prof. Dr J. J. Kelly, Professor of Applied Electrochemistry at the State University of Utrecht, was until recently with Philips Research Laboratories, Eindhoven; J. E. A. M. van den Meerakker, P. H. L. Notten and R. P. Tijburg are with Philips Research Laboratories.

[1] P. Baudet, M. Binet and D. Boccon-Gibod, Low-noise microwave GaAs field-effect transistor, Philips Tech. Rev. **39**, 269-276, 1980.

[2] G. A. Acket, J. J. Daniele, W. Nijman, R. P. Tijburg and P. J. de Waard, Semiconductor lasers for optical communication, Philips Tech. Rev. **36**, 190-200, 1976;
J. C. J. Finck, H. J. M. van der Laak and J. T. Schrama, A semiconductor laser for information read-out, Philips Tech. Rev. **39**, 37-47, 1980.

[3] Special issue 'Compact Disc Digital Audio', Philips Tech. Rev. **40**, 149-180, 1982;
K. Bulthuis, M. G. Carasso, J. P. J. Heemskerk, P. J. Kivits, W. J. Kleuters and P. Zalm, Ten billion bits on a disk, IEEE Spectrum **16**, No. 8 (August), 26-33, 1979.

[4] G. A. Acket, Halfgeleiderlasers voor optische communicatie, Ned. T. Natuurk. B **51**, 13, 1985;
G. A. Acket and W. Nijman, Recente ontwikkelingen op het gebied van halfgeleiders, Ned. T. Natuurk. A **53**, 22-24, 1987.

which, though chemically closely related, are still sufficiently different for a suitable etchant to give a completely different etching behaviour.

In the investigation described in this article we made an extensive study of the etching behaviour of various III-V semiconductors in a variety of aqueous solutions. This was done for each of the three possible etching mechanisms: electrochemical oxidation with an external voltage source ('anodic etching'), electrochemical etching with an oxidizing agent but no external voltage source, known as 'electroless etching', and chemical etching with a reactive compound. The investigation has led to an improved understanding of the processes involved in the different mechanisms. As a result, some new etchants have been developed that can be used to improve the fabrication of the structures for certain applications.

In this article we shall first give a brief description of the three etching mechanisms. We shall then look at some kinetic and crystallographic aspects of etching that are relevant to the production of particular etch patterns. Finally we shall give some examples of wet-chemical etching of III-V semiconductors in practical applications.

Etching mechanisms

Anodic etching

For anodic etching of a III-V semiconductor in an electrolyte the semiconductor is connected to the positive terminal of a direct-voltage source and an inert counter-electrode is connected to the negative terminal. When the potential of the anode is made sufficiently positive a current starts to flow, and the constituent elements become oxidized at the surface of the semiconductor. The ions formed in this process dissolve. The occurrence of oxidation implies that electrons are withdrawn from the valence band of the semiconductor or — and this amounts to the same thing — that holes are supplied to the valence band. In general, the dissolution of a III-V semiconductor (e.g. GaAs) is found to require six holes (h^+) per formula unit [5]:

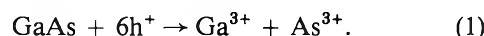

$$GaAs + 6h^+ \rightarrow Ga^{3+} + As^{3+}. \quad (1)$$

The nature of the reaction products depends on the pH-value and composition of the electrolyte. The etching reaction of GaAs in acidic solutions can be represented as follows:

$$GaAs + 3H_2O + 6h^+ \rightarrow Ga^{3+} + H_3AsO_3 + 3H^+. \quad (2)$$

The dependence of the anodic etch rate on the applied potential is determined by the potential distribution at the interface between the semiconductor and the electrolyte. As with a metal electrode, there is a potential difference across a region known as the Helmholtz double layer in the solution near the interface. There is an important difference from a metal electrode, however; the potential drop extends some way into the semiconductor material; see *fig. 1*. Because of this 'space-charge layer', which is formed below the surface as a result of the relatively low concentration of charge carriers in a semiconductor, the energy bands are curved.

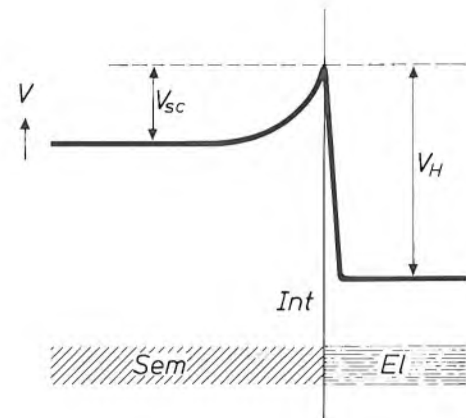

Fig. 1. The potential V at the interface *Int* of a semiconductor *Sem* and an electrolyte *El*. The potential distribution at a semiconductor electrode in an electrolyte differs from that of a metal electrode in that there is not only a potential difference, V_H, across the Helmholtz double layer but also a much more gradual fall in potential, V_{sc}, across the space-charge layer beneath the semiconductor surface.

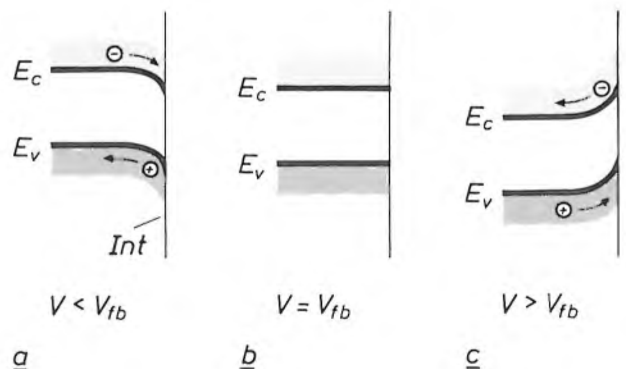

Fig. 2. Energy-level diagram for a semiconductor at the interface *Int* with an electrolyte for different values of the external potential V with respect to the flat-band potential V_{fb}, i.e. the potential at which the energy-band edges are flat right up to the surface. E_v top of the valence band. E_c bottom of the conduction band. The relative movements of electrons in the conduction band and holes in the valence band are also shown. At $V < V_{fb}$ (*a*) the bands are bent downwards; electrons tend to move to the surface and holes tend to move towards the bulk of the semiconductor. At $V = V_{fb}$ (*b*) the concentration of charge carriers at the surface is equal to the concentration in the bulk. At $V > V_{fb}$ (*c*) the bands are bent upwards, so that holes tend to go to the surface and electrons to the bulk. The location of E_v and E_c at the interface does not depend on the band-bending. The Fermi level (not shown) is assumed to be straight; in the bulk it is close to the conduction band if the semiconductor is n-doped and close to the valence band if the semiconductor is p-doped.

When the external potential is varied it is often found that only the potential difference across the space-charge layer changes, while that across the Helmholtz layer remains unchanged [6]. There is a particular potential at which the energy-band edges in the semiconductor go straight to the surface without bending. This potential, known as the 'flat-band potential', V_{fb}, depends not only on the semiconductor material but also on the doping and the nature of the electrolyte.

The effect of the applied potential on the energy bands is shown schematically in *fig. 2*. When the potential is negative with respect to V_{fb} the bands bend downwards. This means that there are more electrons and fewer holes near the surface than in the bulk of the material. At a potential equal to V_{fb} the bands run completely straight: the charge-carrier concentration is the same at the surface as in the bulk. When the potential is positive with respect to V_{fb}, the bands bend upwards: there are then fewer electrons at the surface and more holes than in the bulk.

With n-type doping the value of V_{fb} is lower than with p-type doping. This is because V_{fb} is a measure of the position of the Fermi level in the flat-band situation, and because this level lies close to the conduction band for n-type doping and close to the valence band for p-type doping. The difference in V_{fb} is therefore approximately equal to E_g/e, where E_g is the band gap of the semiconductor and e the electronic charge.

For the oxidation of a III-V semiconductor to take place via the reaction with holes at the surface, there must be a sufficient number of holes in the valence band. This will be the case if the p-type doping is high enough as a result of the incorporation of a sufficient number of acceptor atoms. When there is equilibrium between the charge carriers at the surface and in the bulk the concentration of holes at the surface (p_s) is given by the Boltzmann equation:

$$p_s = p_b \exp(eV_{sc}/kT), \tag{3}$$

where p_b is the concentration in the bulk, V_{sc} the potential drop across the space-charge layer in the semiconductor, k is the Boltzmann constant and T the absolute temperature. Assuming that the potential difference across the Helmholtz layer is constant, it follows from the definition of the flat-band potential that:

$$V_{sc} = V - V_{fb}, \tag{4}$$

where V is the applied potential. It will be clear that the dissolution of a p-doped semiconductor requires a potential approximately equal to V_{fb} (fig. 2*b*) or, better still, positive with respect to V_{fb} (fig. 2*c*).

A measured current-potential curve for p-GaAs is shown in *fig. 3a*. As would be expected, the current and hence the etch rate in the vicinity of V_{fb} increases exponentially with the potential, as a result of the exponential increase in the concentration of holes at the surface; see eq. (3).

Undoped or n-doped semiconductors cannot be directly dissolved anodically, because of the absence of holes in the valence band. In this case, however, we can make use of the effect of illumination on semiconductors. Photons of sufficient energy can excite electrons from the valence band into the conduction band, so that holes are formed in the valence band. If the band-bending within the semiconductor is appropriate, the holes are able to reach the surface and the etching reaction can take place; this is referred to as photo-anodic etching.

Fig. 3*b* shows a current-potential curve for an illuminated n-GaAs electrode in an acidic solution. It

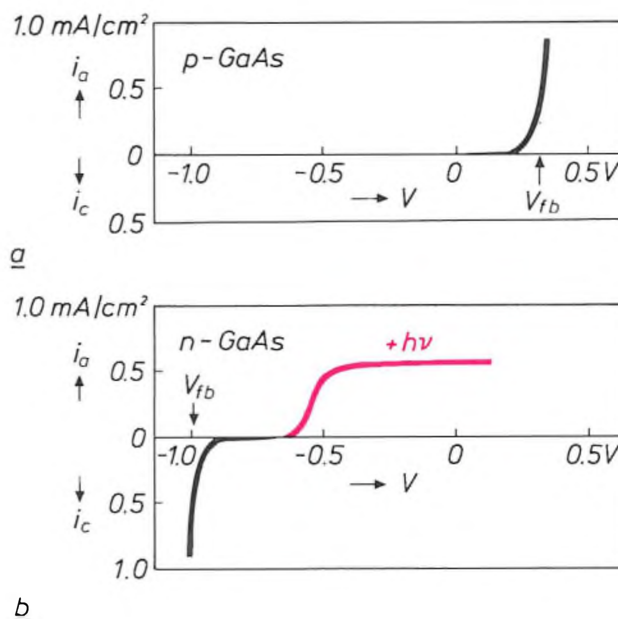

Fig. 3. Current-potential curves for p-GaAs (*a*) and n-GaAs (*b*) in 1N H_2SO_4. The anodic current density i_a and the cathodic current density i_c are plotted against the potential V of the semiconductor electrode with respect to a saturated calomel electrode. With p-GaAs a large potential-dependent anodic current flows as soon as the potential approaches the flat-band value V_{fb}. With n-GaAs a cathodic current flows at low potentials because electrons from the conduction band reduce H^+ ions in the solution to hydrogen gas. In the dark n-GaAs gives no anodic current. An anodic current (red) does flow upon illumination with photons of sufficient energy $h\nu$. This current only starts to flow at a potential that is substantially higher than the flat-band value for n-GaAs, and does not increase further at high potentials.

[5] H. Gerischer, Über den Mechanismus der anodischen Auflösung von Galliumarsenid, Ber. Bunsenges. Phys. Chem. 69, 578-583, 1965.

[6] R. Memming, Energy production by photoelectrochemical processes, Philips Tech. Rev. 38, 160-177, 1978/79.

can be seen that the anodic current associated with the etching only occurs at a potential much higher than the V_{fb} value of n-GaAs. This is because the holes in an n-type semiconductor are the minority carriers. At a potential close to V_{fb}, the electron concentration at the surface is high and the holes recombine with electrons. At a higher potential the electrons and holes are effectively separated by the electric field (fig. 2*c*); the holes are now able to reach the surface and cause dissolution of the semiconductor. At a particular potential the anodic current saturates. In this case all the photo-generated holes take part in the etching process and the anodic current is proportional to the intensity of the incident light.

Anodic etching is not normally the most popular method for semiconductor technology. Working with a voltage source and a counter-electrode, with various electrical contacts, can be very inconvenient. Applying an electrical contact to a semiconductor material during the fabrication process can also be a problem and may even be undesirable for certain applications. There are however circumstances in which other etching methods give poor results and anodic etching may offer success. The study of anodic etching can also supply useful information about electroless etching.

Electroless etching

In electrochemical etching without an external voltage source, 'electroless etching', the etchant contains an oxidizing agent. The dissolution of the semiconductor is due to the oxidizing agent depleting the semiconductor of valence-band electrons and thus in fact supplying it with holes, so that it is itself reduced. A suitable oxidizing agent, e.g. for GaAs, is Ce^{4+}:

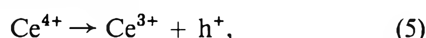

$$Ce^{4+} \rightarrow Ce^{3+} + h^+, \quad (5)$$

where the total reaction can be represented by

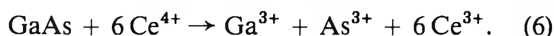

$$GaAs + 6\,Ce^{4+} \rightarrow Ga^{3+} + As^{3+} + 6\,Ce^{3+}. \quad (6)$$

A reaction of this kind is thermodynamically possible only if the redox potential, i.e. the equilibrium potential of the redox couple (in this case Ce^{4+}/Ce^{3+}), is higher than the potential of the solid (GaAs) in equilibrium with 'its ions' (Ga^{3+}, As^{3+}) in the solution. The rate of the reaction depends on the location of the energy bands of the semiconductor in relation to the energy levels of the redox couple in the solution.

Usually, the redox potential is related to the potential of a reference electrode, e.g. a saturated calomel electrode or a standard hydrogen electrode. In solid-state physics, however, the potential of an electron in vacuum is taken as the reference. If we take the same reference for an electrolyte, then the redox potential corresponds to the energy necessary for transferring an electron from the redox couple to vacuum. The energy of the electrons in the solution is then defined in the same way as for those in the solid, so that the redox potential can be considered as the Fermi level of the solution. Because of the interaction of the ions of the redox couple with the solvent, the electron energy of the reduced component is not the same as that of the oxidized component. The energy levels of the oxidized and reduced components are not discrete; they are broadened by the fluctuations of the solvation shell. This results in two Gaussian energy-distribution functions that are symmetrical with respect to the Fermi level, i.e. the redox potential; see *fig. 4*.

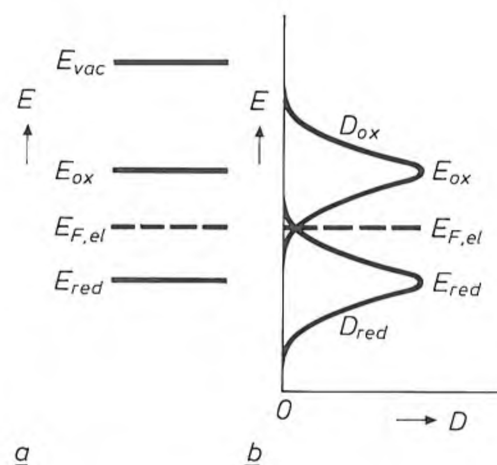

Fig. 4. *a*) Simplified diagram of the energy levels of the components of a redox couple in an electrolyte with respect to the potential energy E_{vac} of an electron in vacuum[6]. Because of the interaction with the solvent, the empty level E_{ox} of the oxidized component is higher than the filled level E_{red} of the reduced component. The Fermi level $E_{F,el}$, corresponding to the redox potential, lies halfway between E_{red} and E_{ox}. *b*) In reality the levels are broadened to energy-distribution functions D_{red} and D_{ox} owing to fluctuations of the solvation shell.

The dissolution reaction of eq. (6), where the redox couple causes the transfer of six holes to the valence band of the III-V semiconductor, is only possible if the energy-distribution function of the oxidized component corresponds approximately to the location of the valence band of the semiconductor. By measuring the electrode impedance, the potentials of the valence-band and conduction-band edges of the semiconductor can be determined with respect to the same reference potential in the solution. In *fig. 5* redox potentials of a number of redox couples in an acidic solution (pH = 0) are compared with the band-edge potentials of three widely used semiconductors: GaP, GaAs and InP. The couple Ce^{4+}/Ce^{3+} has a highly positive redox potential, so that holes can be injected into all three semiconductors. The redox potential of the couple Fe^{3+}/Fe^{2+} is less positive; this couple can

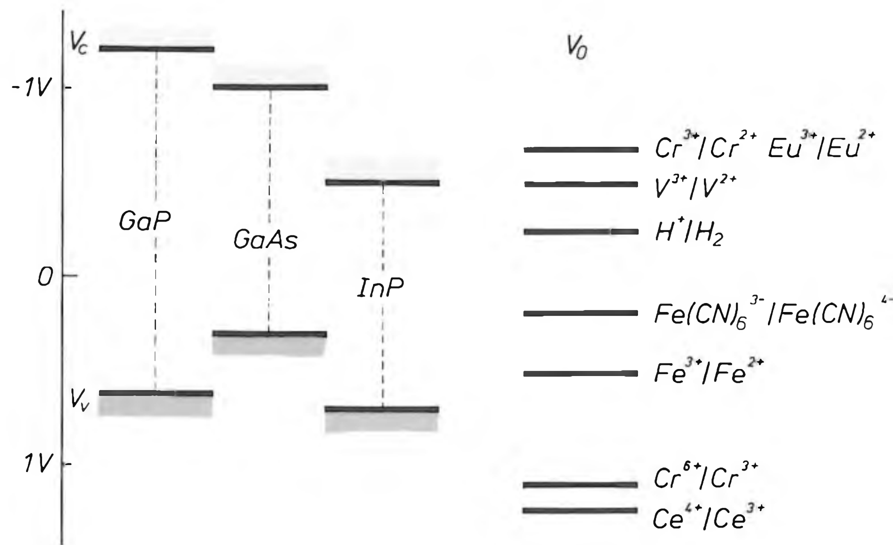

Fig. 5. Potentials of the energy bands of three semiconductors and the redox potentials of a number of redox couples in solutions with a *p*H of 0, measured with respect to a saturated calomel electrode. The potentials of the band edges of the semiconductors are indicated by V_v and V_c. The standard redox potential V_0 is shown for the redox couples; this is the redox potential measured when the concentration of the oxidized component in the solution is equal to that of the reduced component.

still inject holes into GaAs, but not into GaP and InP. The redox potential of the couple $Fe(CN)_6^{3-}$/ $Fe(CN)_6^{4-}$ is such that the injection of holes is no longer possible, not even into GaAs.

Oxidation with a redox couple can be thought of as the sum of an anodic process and a cathodic process, each with its own partial current-potential curve. *Fig. 6* shows these curves for the oxidation of p-GaAs with a Ce^{4+} solution. The anodic partial current increases steeply with the potential, but the cathodic partial current is practically independent of the potential in a wide range. This is because the rate at which the Ce^{4+} ions are reduced is determined entirely by the rate at which they diffuse to the semiconductor surface. Since there is no external current in electroless etching, the etching reaction takes place at the 'mixed potential', where the anodic and cathodic partial currents are equal. The value of the partial currents at the mixed potential determines the etch rate. In this case the etch rate is therefore completely controlled by the diffusion rate of the Ce^{4+} ions in the solution.

Since electroless etching depends on the transfer of electrons from the valence band to the oxidizing agent in the solution, both p-doped and n-doped semiconductors can be dissolved with the same etchants. The current-potential curves differ, however, because the injected holes in n-doped material are minority carriers. As an example, *fig. 7* gives the current-potential curves for n-GaAs in a Ce^{4+} solution. In the range of potentials from -1.0 V to -0.6 V the total current is still equal to the cathodic partial current because of the Ce^{4+} reduction. At these potentials there is not much band-bending, so that the electron concentration is relatively high at the surface and the injected holes recombine with the electrons supplied from the bulk. At higher potentials the electron concentration at the surface becomes negligible and the injected holes can no longer recombine with electrons. The holes then remain at the surface and oxidize the GaAs. Over the entire range of potentials the Ce^{4+} reduction gives the same cathodic partial current, which depends on the diffusion rate of the Ce^{4+} ions. Since at high potentials all the injected holes are used for oxidation, the anodic partial current at such potentials is equal to the cathodic partial current. At the mixed potential the rates of the GaAs oxidation and Ce^{4+} reduction are exactly equal and the recombination rate is zero. The etch rate of n-GaAs is thus determined by the diffusion rate of the Ce^{4+} ions and is the same as that of p-GaAs.

In fig. 5 the band-edge potentials of the semiconductors and the redox potentials of the redox couples apply to acidic solutions ($p\text{H} = 0$). A change in the *p*H-value of the solution has no effect on the redox potential of a couple like $Fe(CN)_6^{3-}/Fe(CN)_6^{4-}$. The presence of H^+ ions or OH^- ions does however have a marked effect on the number of ions adsorbed at the semiconductor surface. This changes the potential difference across the Helmholtz layer (fig. 1), resulting in a different flat-band potential. It is known that the flat-band potential decreases by about 60 mV per unit increment in the *p*H. This means that at a *p*H of 14

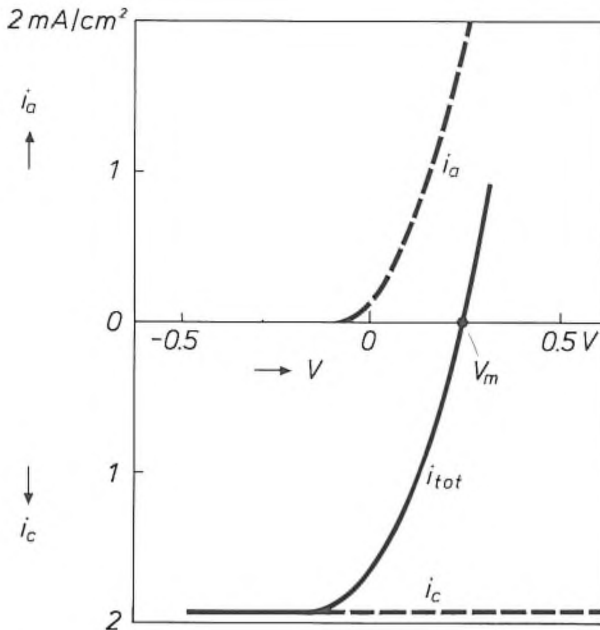

Fig. 6. Current-potential curves for p-GaAs in a Ce^{4+} solution. The anodic partial current density i_a due to the GaAs oxidation, the cathodic partial current density i_c due to the Ce^{4+} reduction, and the total current density i_{tot} are shown, plotted against the potential V with respect to a saturated calomel electrode. Whereas i_a at a particular potential increases steeply with V, the value of i_c is practically independent of the potential in a wide range. The electroless etching takes place at the mixed potential V_m, where $i_a = i_c$. In this case the etch rate, which is proportional to the value of i_a at V_m, is determined entirely by the constant cathodic partial current.

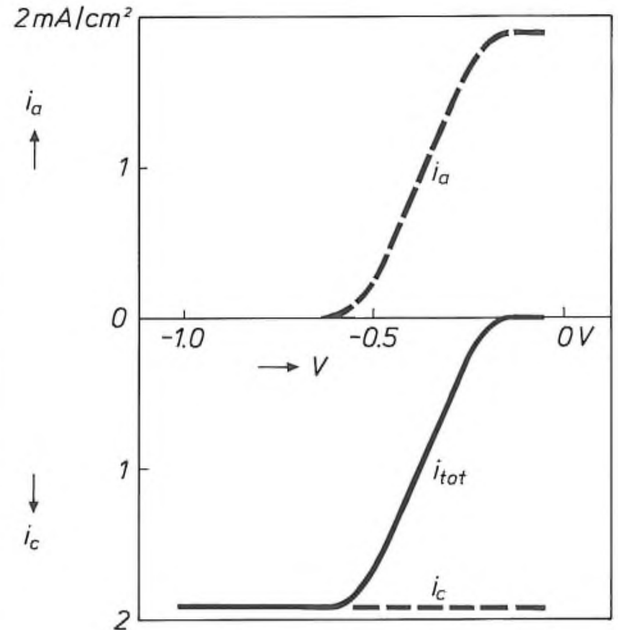

Fig. 7. Current-potential curves (as in fig. 6) for n-GaAs in a Ce^{4+} solution. Here again i_c is constant but i_a also becomes constant at high potentials and practically equal to i_c. The value of i_c again determines the etch rate.

the band-edge potentials of the semiconductors are shifted upwards by about 0.8 V with respect to those in fig. 5. The redox potential of $Fe(CN)_6^{3-}/Fe(CN)_6^{4-}$, for example, then comes to lie below the valence-band-edge potentials of GaP, GaAs and InP. The result is that this couple can inject holes into the valence band of all three semiconductors, so that etching is in fact possible at a *p*H of 14.

A redox potential that is well placed with respect to the valence-band-edge potential of the semiconductor is not always a guarantee of a satisfactory etching reaction. At the surface of InP, for instance, the reduction of Ce^{4+} is inhibited to such an extent, probably due to the formation of a thin oxide film, that there is hardly any etching. Etching GaAs with CrO_3/HF solutions is also less effective. In spite of the appropriate redox potential of the Cr^{6+}/Cr^{3+} couple, the dissolution rate of the GaAs is much lower than would be expected from the diffusion rate of Cr^{6+}. In this case the semiconductor surface is partly passivated by the adsorption of an intermediate formed during the etching reaction, probably a complex of hexavalent and trivalent chromium [7].

Besides the oxidizing agents that can give an etching reaction in the dark, there are other agents that can

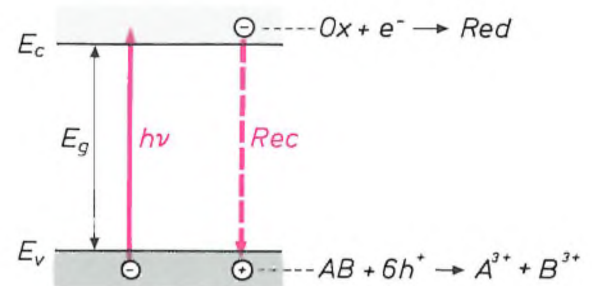

Fig. 8. Principle of electroless photo-etching of a III-V semiconductor AB. Photons of energy $h\nu$ equal to or greater than the band gap E_g excite electrons from the valence band to the conduction band. The holes formed oxidize the semiconductor while the electrons in the conduction band reduce the oxidizing agent Ox to Red. A competing process is the recombination *Rec* of electrons and holes.

etch III-V semiconductors under illumination. This 'photo-etching' depends on both majority and minority carriers; see *fig. 8*. Photons with an energy equal to or greater than the band gap of the semiconductor generate electron-hole pairs. The holes that are formed oxidize the semiconductor, while the electrons reduce the oxidizing agent. A competing process is the recombination of electrons and holes. The couples that would appear to be useful for the photo-etching are those whose redox potential lies above the valence-band potential of the semiconductor and whose oxidized component has an energy-distribution function that corresponds to the conduction band. In the case of GaAs, for example, these are the couples V^{3+}/V^{2+},

Cr^{3+}/Cr^{2+} and Eu^{3+}/Eu^{2+} (fig. 5). We have found however that these couples are unsuitable for photo-etching III-V semiconductors, because the electron transfer to the oxidizing agent cannot compete with the electron-hole recombination. There are some more complicated redox couples that do provide effective electron transfer [8], however. Acidic H_2O_2 solutions, for example, can be used to photo-etch both p-type and n-type GaAs [9]. We shall not consider the intricate mechanism of these etching reactions here.

Chemical etching

Chemical etching does not involve free charge carriers and cannot therefore be affected by an external potential. In chemical etching the surface of the semiconductor is attacked through the action of reactive molecules (e.g. HCl), with the result that bonds between the surface atoms are broken and at the same time new bonds are formed with the atoms of the reactive molecules. The compounds formed dissolve in the etchant or escape as gases.

A mechanism of this type is found in the etching of InP with concentrated HCl solutions [10]. Since the dissolution of InP is due to the reaction with undissociated HCl molecules, the HCl concentration has to be fairly high — higher than 6 M at room temperature. The concentration can be lower in a solution containing a large amount of acetic acid, because the dissociation content of HCl is smaller in such a solution [11].

In the reaction between InP and HCl it is likely that a bond between In and P is broken at the same time as the bond between H and Cl, and that new bonds are then formed between In and Cl and between P and H:

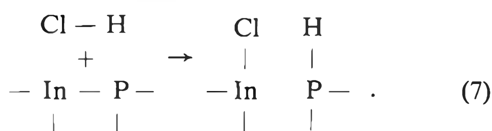

(7)

Since each surface atom is bonded to three atoms below it, two bonds then remain to be broken. Finally, the indium dissolves as $InCl_3$, while the phosphorus disappears as PH_3:

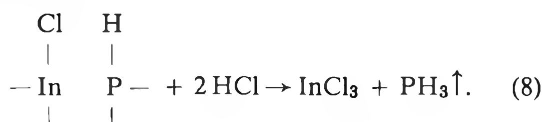

(8)

In some cases the etching mechanism may be changed by the action of light. An example is found in the etching of GaAs with H_2O_2 solutions. In the dark only a chemical mechanism is active, but illumination gives rise to an electrochemical etching process, in which the holes formed in the valence band oxidize the GaAs [8].

Kinetic and crystallographic aspects

The rate at which III-V semiconductors are dissolved by a particular etching mechanism depends on a number of factors. The rate, for example, may be determined entirely by the kinetics of the reaction at the semiconductor surface. However, if the rate of this reaction is very high, the rate-determining parameter may be mass transfer in the solution. The etch rate may also be very dependent on the crystallographic orientation of the surface. Etching near the edges of masks may produce special effects. If a semiconductor is being etched in contact with another semiconductor or a metal, it might be expected that the rate of dissolution would be affected by the galvanic interaction between the materials. Since all these factors are relevant to the practical applications to be discussed, we shall first take a closer look at them.

Rate-determining step

In a kinetically controlled etching process, where the surface reaction is rate-determining, the concentration of the rate-determining species at the surface (c_s) will be equal to that in the bulk of the solution (c_b). In the simplest approximation the etch rate r_k is then given by

$$r_k = k\, c_b^n, \qquad (9)$$

where k is the reaction-rate constant and n the order of the reaction. The rate constant is given by:

$$k = A \exp(-E_a/RT), \qquad (10)$$

where A is a constant, E_a the activation energy for the reaction, R the gas constant and T the absolute temperature. A plot of log r_k against $1/T$ gives a straight line. The activation energy that can be derived from the slope of this line is of the order of 40 kJ/mol for most kinetically controlled etching reactions. This means that the activation energy per molecule is of the order of 0.4 eV.

[7] J. van de Ven, J. E. A. M. van den Meerakker and J. J. Kelly, The mechanism of GaAs etching in CrO_3-HF solutions, I. Experimental results, J. Electrochem. Soc. **132**, 3020-3026, 1985;
J. J. Kelly, J. van de Ven and J. E. A. M. van den Meerakker, The mechanism of GaAs etching in CrO_3-HF solutions, II. Model and discussion, J. Electrochem. Soc. **132**, 3026-3033, 1985.

[8] J. J. Kelly, J. E. A. M. van den Meerakker and P. H. L. Notten, Electrochemistry of photo-etching and defect-revealing in III-V materials, in: Grundlagen von Elektrodenreaktionen, Dechema Monographien, Band 102, VCH Verlagsgesellschaft, Frankfurt am Main 1986, pp. 453-464.

[9] D. V. Podlesnik, H. H. Gilgen and R. M. Osgood, Jr, Deep-ultraviolet induced wet etching of GaAs, Appl. Phys. Lett. **45**, 563-565, 1984.

[10] P. H. L. Notten, The etching of InP in HCl solutions: a chemical mechanism, J. Electrochem. Soc. **131**, 2641-2644, 1984.

[11] W. Huber, Titrations in non aqueous solvents, Academic Press, New York 1967, p. 215 and 226.

In an etching process with a very high rate constant the concentration of the reagent at the semiconductor surface may be so low that the diffusion of the reagent to the surface will be rate-determining. The rate of a diffusion-controlled etching process (r_d) is proportional to the concentration gradient at the surface. For one-dimensional diffusion with a linear concentration gradient it is given approximately by

$$r_d \approx \frac{D}{\delta}(c_b - c_s), \qquad (11)$$

where D is the diffusion coefficient and δ the thickness of the 'diffusion layer' at the surface. The temperature dependence of the etch rate is now mainly determined by that of the diffusion coefficient, which is inversely proportional to the viscosity of the solution. For the aqueous solutions normally used we can derive an 'activation energy' of about 18 kJ/mol from the curve of log r_d against $1/T$.

If the rate of the surface reaction is of the same order of magnitude as the rate of diffusion, there are various methods for influencing the rate-determining step. In the case where the surface reaction is not of the first order ($n > 1$), it follows from eq. (9) that increasing the concentration c_b will result in a greater increase in the reaction rate, so that the diffusion becomes more important. A change in the same direction is obtained by increasing the temperature; see *fig. 9*. The surface reaction, which is rate-determining at low temperatures, is much more temperature-dependent than the diffusion, so that at higher temperatures the diffusion becomes the rate-determining quantity. A change in the opposite direction can be obtained by reducing the thickness δ of the diffusion layer; see eq. (11). This can be done by rotating the semiconductor or by stirring the solution. It is then possible to change a diffusion-controlled process into a kinetically controlled process.

Diffusion in electroless etching

In the example given in fig. 6 the anodic partial current due to the oxidation of GaAs is kinetically controlled. The current depends only on the hole concentration at the surface. Near the mixed potential the reduction rate is determined by the diffusion of the oxidizing agent (Ce^{4+}) to the surface. This means that the rate of the total process is determined by diffusion via the reduction reaction. This situation is most frequently encountered in electroless etching.

We have been able to show that the etch rate can also be determined by diffusion via the oxidation reaction. This is illustrated in *fig. 10* for p-GaAs in a solution of 0.5 M $K_3Fe(CN)_6$ with a *p*H of 13. The total current-potential curve has three distinct plateaus. At low potentials the cathodic partial current due to the reduction of $Fe(CN)_6^{3-}$ is entirely determined by diffusion and does not depend on the potential. The reduction stops as soon as the potential approaches the redox potential of the $Fe(CN)_6^{3-}/Fe(CN)_6^{4-}$ couple. The anodic partial current due to the GaAs oxidation becomes important at the flat-band potential. At higher potentials, however, the anodic partial current also becomes constant. We have found that the etching process then depends on the transfer of OH^- ions to the semiconductor surface. The intermediate plateau in the total curve is the result of the difference between the potential-independent sections of the anodic and cathodic partial curves.

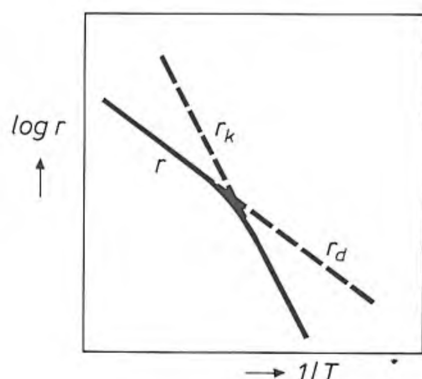

Fig. 9. Diagram showing the effect of the temperature T on the rate r and the kinetics of the etching process, where r_k is the etch rate when the surface reaction is kinetically controlled and r_d is the etch rate when the surface reaction is diffusion-controlled. Both log r_k and log r_d decrease linearly with $1/T$. At low temperatures, however, r_k is much smaller than r_d, so that the surface reaction determines the etch rate ($r = r_k$). At high temperatures r_k is much larger than r_d, and diffusion is then rate-determining ($r = r_d$).

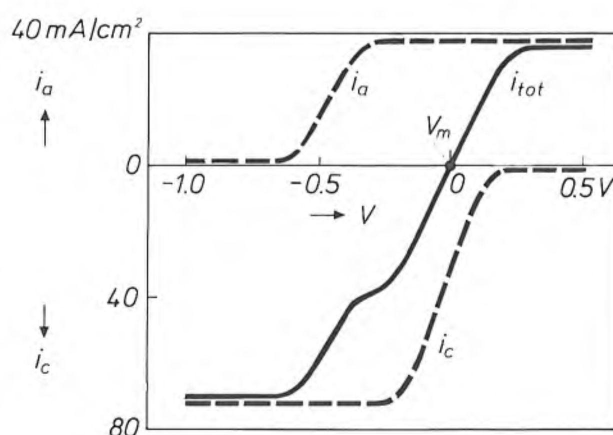

Fig. 10. Current-potential curves (as in figs 6 and 7) for p-GaAs in an 0.5M $K_3Fe(CN)_6$ solution with a *p*H of 13. The anodic and cathodic partial current densities i_a and i_c are such that the curve for the total current density i_{tot} has three plateaus, corresponding to the constant value of i_c at low V, the constant value of i_a at high V and the difference between these two values. The etch rate, which is proportional to i_a at the mixed potential V_m, is not determined by a constant cathodic current in this case, but by a constant anodic current.

The constant cathodic current in fig. 10 is much higher than the constant anodic current. At the mixed potential it is not the cathodic current that is constant, but the anodic current, so that the etch rate is diffusion-controlled via the oxidation reaction. If the $K_3Fe(CN)_6$ concentration is decreased so as to make the constant cathodic current lower than the constant anodic current, the result, just as in fig. 6, is an etch rate that is diffusion-controlled via the reduction reaction.

Effect of the crystal planes

Semiconductors like GaAs, GaP and InP are normally used in single-crystal form. Their crystal structure corresponds to the zinc-blende structure of ZnS. The A atoms (Ga, In) form a face-centred cubic structure in which half the tetrahedral interstices are periodically filled with B atoms (As, P). Crystal planes such as the {100} and {111} planes can be distinguished from each other by a different density and arrangement of the atoms, which can affect the etch rate. Because of the polarity in the ⟨111⟩ directions, an A{111} plane, i.e. a {111} plane occupied only by A atoms, will behave differently from a B{111} plane [12].

The arrangement of the atoms in the surface crystal plane can have a considerable effect on the flat-band potential V_{fb}. *Table I* gives the values of V_{fb} for the {100}, As{111} and Ga{111} planes of n-type and p-type GaAs. The difference in V_{fb} between corresponding crystal planes of n-type and p-type GaAs is approximately equal to E_g/e, where E_g is the band gap of GaAs (see p. 63). The {100} and As{111} planes have almost the same V_{fb}-value, but that of a Ga{111} plane is much higher. Partly because of this the anodic dissolution of a Ga{111} surface only starts at a potential more than 100 mV higher than the onset potential for dissolution of an As{111} surface.

Table I. Flat-band potential V_{fb} with respect to a saturated calomel electrode for three kinds of crystal planes of n- and p-GaAs in an NaOH solution with a *p*H of 14.

Crystal planes	V_{fb}	
	n-GaAs	p-GaAs
{100}	− 1.80 V	− 0.50 V
As{111}	− 1.75	− 0.45
Ga{111}	− 1.55	− 0.25

In the literature various examples are given of the effect of the crystal planes on the rate of chemical etching, when this is not determined by mass transfer in the solution. It was found, for example, in the etching of InP [13] that the rate varies in the sequence P{111} ⩾ {100} ≫ In{111}. The explanation for this goes beyond the scope of this article [12].

Etching at mask edges

If the etch rate is determined by diffusion for all crystal planes, isotropic etching would be expected at mask edges. Chemical etching does indeed give rounded profiles in this case. At a mask edge the etch depth is relatively large, because there is mass transfer both from the solution above the etched surface and from the solution beside the mask aperture. *Fig. 11* shows a profile produced at a mask edge after a diffusion-controlled chemical etching process. It agrees well with the theoretical profile calculated from a two-dimensional model [14].

If the etch rate of one of the crystal planes is determined by the rate of the surface reaction, facets are found at mask edges. The shape of the etch profile is then usually determined by the plane etched most slowly, which is usually an A{111} plane.

In electroless etching processes, profiles with facets may be observed even though the etch rate of all the

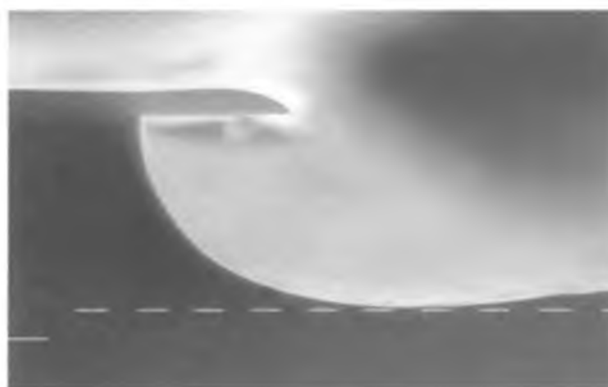

Fig. 11. Scanning electron-microscope photograph (scale divisions 1 µm) of GaAs at a mask edge after a diffusion-controlled etching process with an H_2O_2/HCl solution. The etching results in a rounded profile, in good agreement with a profile calculated for this case [14].

[12] See for example H. C. Gatos, Crystalline structure and surface reactivity, Science **137**, 311-322, 1962.
[13] R. Becker, Sperrfreie Kontakte an Indiumphosphid, Solid State Electron. **16**, 1241-1249, 1973.
[14] H. K. Kuiken, J. J. Kelly and P. H. L. Notten, Etching profiles at resist edges, I. Mathematical models for diffusion-controlled cases, J. Electrochem. Soc. **133**, 1217-1226, 1986;
P. H. L. Notten, J. J. Kelly and H. K. Kuiken, Etching profiles at resist edges, II. Experimental confirmation of models using GaAs, J. Electrochem. Soc. **133**, 1226-1232, 1986.

individual planes is determined entirely by diffusion. This is related to the effect of cathodic protection, which we shall now briefly discuss.

Cathodic protection

When a metal is in contact with another metal during etching, the etch rates of the individual metals may be changed considerably by galvanic effects [15]. The etch rate of the less-noble metal tends to increase, while the more-noble metal is etched more slowly. The more-noble metal is then said to be 'cathodically protected'.

This effect is also found in the electroless etching of different semiconductors or semiconductor regions in contact with each other [16]. *Fig. 12* gives a schematic representation of the current-potential curves for two p-doped III-V semiconductors, A_1B_1 and A_2B_2, of equal area. Owing to the difference in 'nobility' the anodic partial curves of A_1B_1 and A_2B_2 are different. On the other hand the cathodic partial curves coincide, because the reduction rate is assumed to be determined by the diffusion rate of the oxidizing agent in the solution. Consequently the separate semiconductors are etched at the same rate, A_1B_1 at the mixed potential V_1 and A_2B_2 at the mixed potential V_2. If

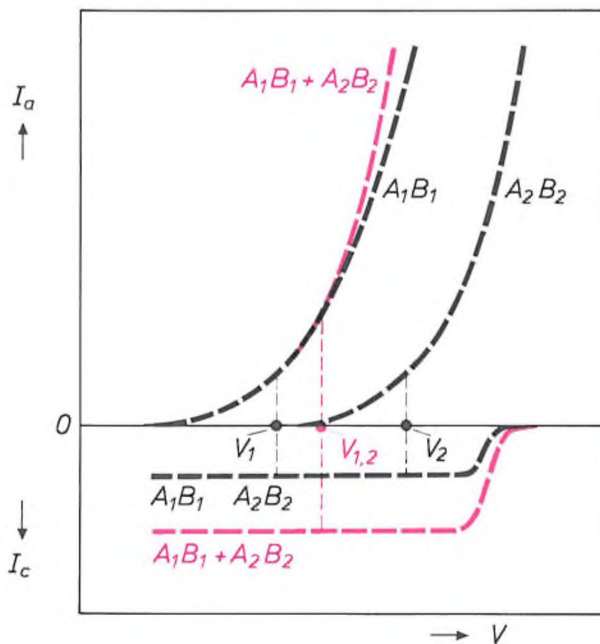

Fig. 12. Schematic current-potential curves illustrating the occurrence of cathodic protection in the etching of two semiconductors in electrical contact. Electroless etching of the individual semiconductors A_1B_1 and A_2B_2 at the mixed potentials V_1 and V_2 takes place at the same rate, determined by the constant value of the cathodic partial current. If there is electrical contact the partial currents of A_1B_1 and A_2B_2 have to be added together (red). Etching then takes place at an intermediate mixed potential, $V_{1,2}$, so that the 'less-noble' A_1B_1 is dissolved faster and the 'nobler' A_2B_2 more slowly.

A_1B_1 and A_2B_2 are in electrical contact, their partial current-potential curves have to be added together. This results in a new curve for the anodic process and in a cathodic current that is twice as large, because the areas of A_1B_1 and A_2B_2 are combined. This gives a new mixed potential ($V_{1,2}$), with a value higher than V_1 and lower than V_2, which means that the etch rate of A_1B_1 is higher and that of A_2B_2 lower.

Cathodic protection can be useful for selectively etching semiconductors in multilayer structures: while there is little or no difference in the etching behaviour of the separate materials, there can be a considerable difference in etch rate because of the electrical contact between them.

Practical examples

The applications of wet-chemical etching of III-V semiconductors are much too numerous for a detailed description of each. We shall therefore confine ourselves to a few interesting applications that we have investigated.

Material quality control

Although the semiconductors used for making electronic devices are true single crystals, they always have some crystallographic defects. These defects, which may decide the quality and life of a component, can be revealed by a treatment with a defect-selective etchant. Defects usually correspond to crystallographically perturbed areas such as dislocations and stacking faults. Since these areas will behave less 'nobly' than their environment, they can be selectively etched in the dark. The higher etch rate at defects leads to the formation of etch pits. The sensitivity of etchants based on this principle is in general low: to make all the defects visible it is necessary to etch away more than 10 μm. Obviously this cannot be done for thin films.

Crystallographic defects can also be revealed by photo-etching, since it is known that effective recombination of free electrons and holes often takes place at such defects. Since the photo-etch rate depends on the surface concentration of both types of charge carrier, the increased recombination at crystal defects produces a local decrease in the etch rate. Photo-etching therefore makes the sites with defects stand out from their environment ('hillocks'). The high sensitivity that can be achieved in this way is demonstrated in *fig. 13*, which shows a photomicrograph of n-GaAs after photo-etching with an H_2O_2/H_2SO_4 solution. Many defects are visible after removal of 0.4 μm of the surface. Striations due to areas of different doping concentration also appear, as parallel lines.

Fig. 13. Photomicrograph (interference contrast) of n-GaAs after photo-etching with an H_2O_2/H_2SO_4 solution for revealing crystal defects[8].

The CrO_3/HF solutions mentioned earlier are also suitable etchants for the quality control of III-V semiconductors. In these etchants the crystallographic defects are revealed by the formation in the dark of a thin passivating film, which is slightly thicker at the defects than on a perfect surface[7]. The defects are thus preferentially passivated, so that they are etched away more slowly. In n-GaAs and n-InP the sensitivity can be increased further by illumination; this effect can again be attributed to increased recombination of electrons and holes at the defects.

Profile etching

The etching of special shapes and profiles with the aid of a resist is a very important process in III-V semiconductor technology. To take a particular example, structures with symmetrically rounded edges or grooves with a V-shaped cross-section are frequently used for semiconductor lasers. Good use can often be made here of etching kinetics. As we have shown, etching processes with a rate-determining surface reaction give structures with facets, whereas the diffusion-controlled chemical etching processes are isotropic. We have also shown that the etching kinetics can be changed, for example by raising the temperature (fig. 9). This makes it possible to influence the etching profile fairly easily. *Fig. 14* shows an example in which the profiles were made in GaAs by chemical etching at different temperatures. At 0 °C the surface reaction is still rate-determining and a V-groove is produced. At 20 °C diffusion becomes important,

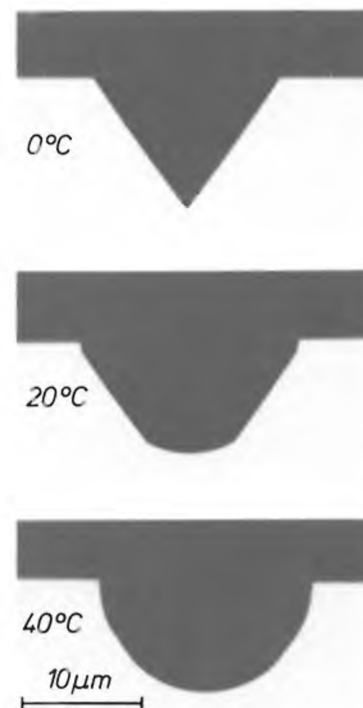

Fig. 14. Photomicrographs of profiles in GaAs after chemical etching with a Br_2/KBr solution at different temperatures. A change in temperature has a pronounced effect on the etching kinetics and gives a completely different etching profile: from a V-groove at 0 °C to an almost completely rounded profile at 40 °C.

with the result that the profile is slightly rounded. At 40 °C diffusion is rate-determining and the result is an almost completely rounded profile.

Another factor that has an important bearing on the shape of the etching profile is the orientation of the mask in relation to the crystal orientation. If for example a narrow track in the $[\bar{1}10]$ direction is etched into a (001) surface, the result is a channel with a V-shaped cross-section, formed by two {111} planes

[15] J. J. Kelly and C. H. de Minjer, An electrochemical study of undercutting during etching of duplex metal films, J. Electrochem. Soc. 122, 931-936, 1975;
J. J. Kelly and G. J. Koel, Galvanic effects in the wet-chemical etching of metal films, Philips Tech. Rev. 38, 149-157, 1978/79.

[16] H. Löwe and I. Barry, Zur Kinetik der Germaniumauflösung in alkalischen Hexacyanoferrat-III-Lösungen, Z. Phys. Chem., Leipzig 249, 73-80, 1972.

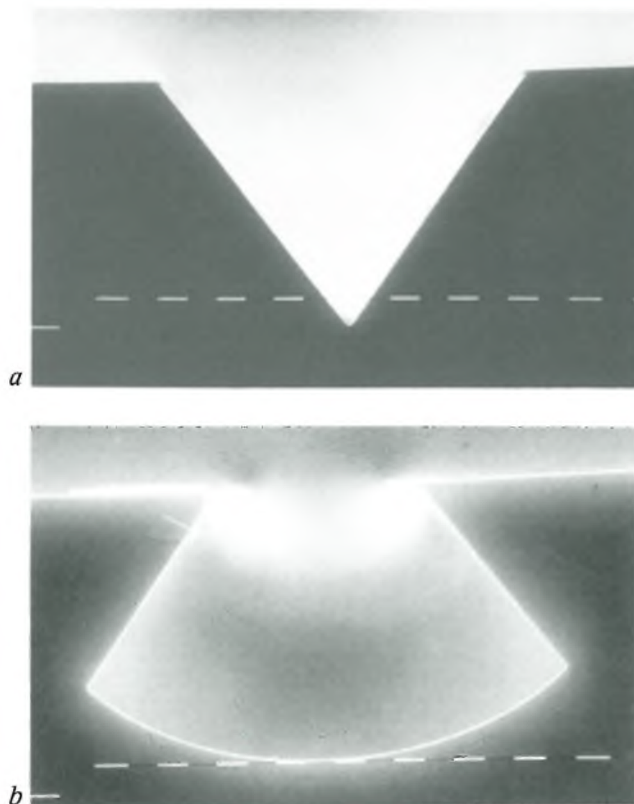

Fig. 15. Scanning electron-microscope photographs (scale divisions 1 μm) of GaAs after chemical etching with a Br_2/HBr solution for two different mask orientations. When a narrow track is etched in the [110] direction a V-groove is formed (*a*). When this is done in the [110] direction, the result is a 'dovetail' (*b*).

with A atoms; see *fig. 15a*. The characteristic etching angle between the side planes and the surface is 55°, corresponding to the angle between the (001) plane and the {111} planes. If on the other hand a narrow track is etched in the [110] direction (i.e. perpendicular to the [$\bar{1}$10] direction), then the etching spreads outwards with a characteristic angle of 125°, corresponding to the supplement of the angle between the (001) plane and the {111} planes. This results in a channel with a 'dovetail' cross-section (fig. 15*b*).

In electroless etching the etch rates for the various crystal planes are clearly often diffusion-controlled, and yet profiles with facets are obtained. In these cases the etch rate is determined by the cathodic partial current due to the reduction reaction (figs 6 and 7). During etching at a mask edge various crystal planes are exposed to the etchant. As we have shown, these have different V_{fb}-values (Table I) and the anodic-current-potential curve depends on the crystal plane. This means that galvanic effects can occur between the planes of *the same* crystal. In an analogous way to that shown in fig. 12, the most-noble plane is cathodically protected by the rest of the surface, and this results in the formation of a facet.

This effect does not occur when, as in fig. 10, the etch rate is determined by a diffusion-controlled anodic current. This situation is shown schematically in *fig. 16*. In this case the diffusion-controlled cathodic current (not shown) is very high and there are two planes of quite different nobility. It can be seen from the anodic current at the mixed potential that the electrical contact between the planes has no effect on their etch rate. There is no cathodic protection, so that the planes dissolve at the same diffusion-controlled rate and a rounded profile is obtained.

In the photo-etching of III-V semiconductors using light of very short wavelength (e.g. 350 nm) an exceptionally high anisotropy can be achieved [9]. The strong absorption of the light induces a relatively high concentration of holes in the exposed part of the semiconductor surface, resulting in a highly direction-dependent etching process. Since the etched cavity acts as a waveguide for the incident light, and dissolution only occurs at the bottom of the cavity, structures with very deep holes or grooves can be produced. Structures of this type offer interesting prospects for practical application.

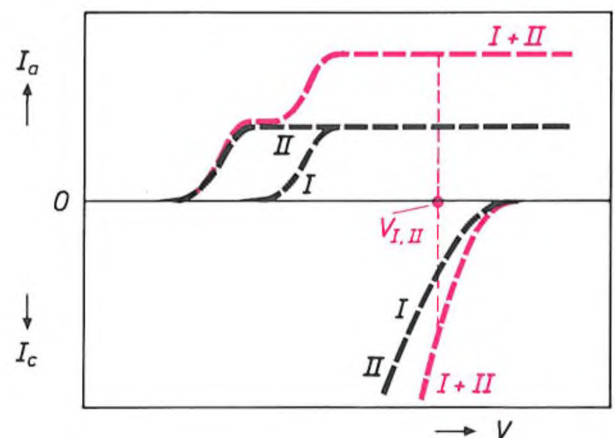

Fig. 16. Schematic current-potential curves for the etching of two crystal planes *I* and *II*, of dissimilar 'nobility', with no cathodic protection. Both planes give the same diffusion-controlled constant anodic current, which is much lower than the diffusion-controlled cathodic current (not shown here). At the mixed potential $V_{I,II}$ the total anodic current (red) is equal to the sum of the constant anodic currents of *I* and *II*, so that the electrical contact between *I* and *II* has no effect on their etch rates.

Selective etching

In III-V semiconductor technology there is a need for selective etchants that are highly sensitive to the composition of the material. High selectivity is particularly important for etching thin-film structures, as in semiconductor lasers, in which the active layer is no thicker than 0.1 μm. To illustrate what can be achieved in this field we shall discuss a few typical examples.

With chemically dissimilar materials the required selectivity can often be obtained by using the appropriate etchant. For instance, InP can be dissolved selectively with respect to $In_xGa_{1-x}As_yP_{1-y}$ by chemical etching in a concentrated HCl solution, in which the $In_xGa_{1-x}As_yP_{1-y}$ is hardly attacked at all. *Fig. 17* shows a multilayer structure with these semiconductors, in which the InP has been partly removed by selective etching. The opposite selectivity can be obtained in electroless etching, e.g. with a Ce^{4+}/H_2SO_4 solution. The $In_xGa_{1-x}As_yP_{1-y}$ readily dissolves in this solution, while the InP is passivated, probably because of the formation of an oxide film on the surface. An example of a multilayer structure etched in this way is shown in *fig. 18*.

Both forms of selectivity are also possible with GaAs and $Al_xGa_{1-x}As$. In etching multilayer structures with these materials the $Al_xGa_{1-x}As$ is passivated to such an extent in some solutions, by the formation of an oxide film, that virtually only the GaAs is attacked; see *fig. 19*. A suitable method for selectively dissolving $Al_xGa_{1-x}As$ with respect to GaAs is based on the difference in the nobility of these compounds in electroless etching. *Fig. 20* shows a multilayer structure treated by this method. Etching through a mask first produces a narrow hole in the upper GaAs layer, and then a much wider hole in the $Al_xGa_{1-x}As$ layer beneath it. The bottom GaAs layer is not attacked, however, because of its greater nobility and the cathodic protection.

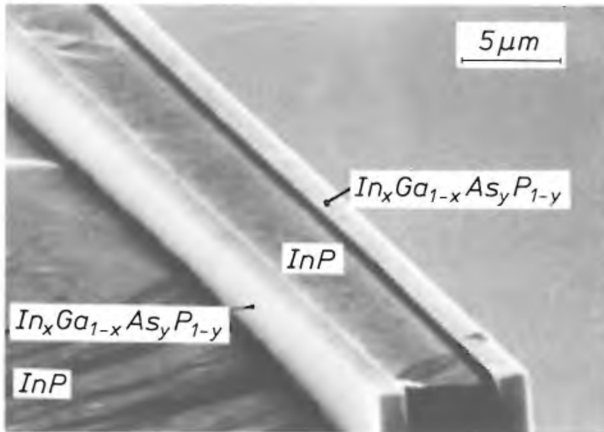

Fig. 17. Scanning electron-microscope photograph of a multilayer structure of InP and $In_xGa_{1-x}As_yP_{1-y}$, after chemical etching with a concentrated HCl solution. Only the InP layers have been partly etched away.

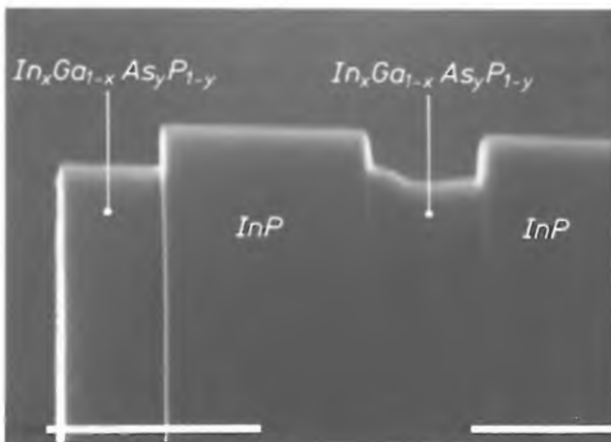

Fig. 18. Scanning electron-microscope photograph (scale divisions 1 µm) of a multilayer structure of InP and $In_xGa_{1-x}As_yP_{1-y}$, in which electroless etching with a Ce^{4+}/H_2SO_4 solution has only affected the $In_xGa_{1-x}As_yP_{1-y}$.

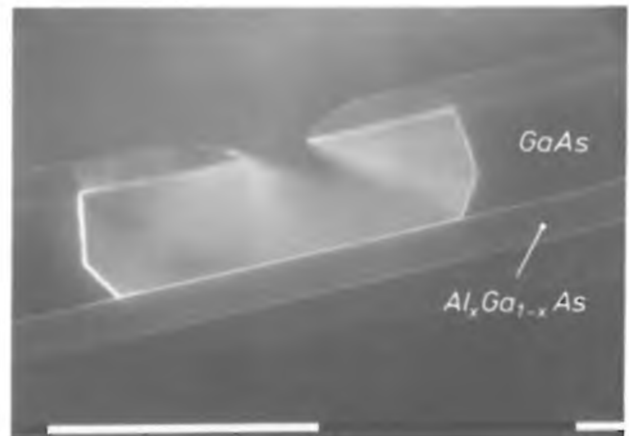

Fig. 19. Scanning electron-microscope photograph (scale divisions 1 µm) of a multilayer structure of GaAs and $Al_xGa_{1-x}As$, in which only GaAs has been partly removed by chemical etching with an H_2O_2 solution.

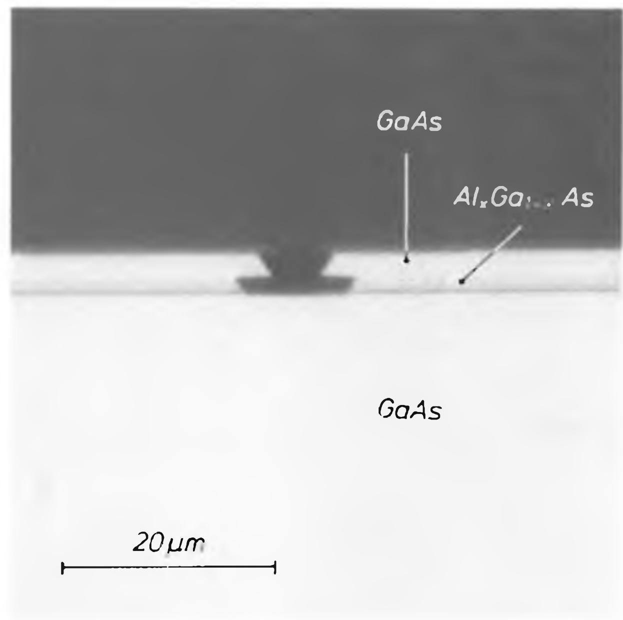

Fig. 20. Photomicrograph of a multilayer structure of GaAs and $Al_xGa_{1-x}As$. Electroless etching through a mask has produced a relatively small hole in the top GaAs layer and a much wider hole in the underlying $Al_xGa_{1-x}As$ layer. The bottom GaAs layer has not been attacked, however.

The selective etching of semiconductor materials that differ only in the type of doping is in general not possible by electroless or chemical etching. Although some selectivity may be obtained with electroless photo-etching, the most reliable method is based on anodic etching. The principle can be simply illustrated with reference to fig. 3. The p-GaAs is selectively dissolved in the dark at a potential near its flat-band potential (about 0.3 V), whereas on exposure to light and with a lower potential only the n-GaAs is dissolved. In this way regions on either side of a pn-junction in GaAs can be etched selectively. A p-doped InP layer can also be completely removed from an n-InP layer beneath it by anodic etching.

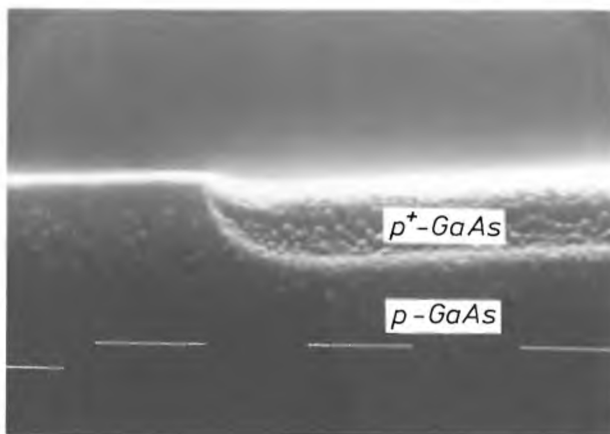

Fig. 21. Scanning electron-microscope photograph (scale divisions 1 μm) of a GaAs layer in which the heavily doped p^+ region has been etched away with a $K_3Fe(CN)_6$ solution; the less heavily doped p region has hardly been attacked.

By using a difference in potential distribution, with cathodic protection, we have succeeded in selectively etching semiconductor materials that differ only in doping concentration. Such combinations of materials are found in laser structures with a top layer of p-GaAs that is heavily doped (p^+) locally to give good electrical contact. The contact region can be revealed by selective etching with a solution of 0.1 M $K_3Fe(CN)_6$ at a *p*H of 14; see *fig. 21*. The only difference between the p and p^+ regions shown here is the doping concentration: 10^{18} and 10^{20} cm^{-3}. Because of the near-metallic nature of the p^+ region, the potential distribution at the interface with the solution is quite different from that for a conventional p-type semiconductor. The p^+ region is less noble and is more rapidly dissolved when in contact with a large p-type area.

Summary. III-V semiconductors like GaAs can be wet-chemically etched by three mechanisms: electrochemically with an external voltage source, electrochemically using an oxidizing agent (electroless), and chemically with a reactive compound. In some cases the etching process only proceeds when the semiconductor is exposed to light. The etch rate depends on the relative reaction rate at the semiconductor surface and the mass transfer in the solution. Other important factors are the effect of the crystal planes, the orientation of a mask with respect to these planes, and the electrical contact with other materials. Wet-chemical etching of III-V semiconductors can be used on a large scale for various applications, including the detection of crystallographic defects, the fabrication of special profiles and the selective dissolution of closely related materials in multilayer structures.

1938 THEN AND NOW 1988

Lamps for phototherapy

The treatment of certain complaints by radiation with artificial light (phototherapy) first became known in about 1900. The method grew in importance as new kinds of lamps were invented and as promising results were obtained with solar radiation. Artificial light freed the therapeutist from the uncertainties of the weather, and the radiation could be kept to a narrow wavelength range to give a better therapeutic action with fewer harmful side effects.

It is about fifty years since Philips developed the 'Biosol' lamp for ultraviolet radiation [*] (black-and-white photograph). This was a tubular discharge lamp with a length of about 20 cm, a gas pressure of 1 bar and a power of 250 or 475 W. The lamp was intended for the treatment of diseases such as rickets, with radiation at a wavelength of about 250 nm, and lupus (tuberculosis of the skin), at a wavelength of 320 to 350 nm. Filters gave a wavelength distribution as close to the ideal as possible.

With the passage of time, progress in lighting technology and our improved understanding of phototherapy have enabled us to match the wavelength more closely to the ailment. One important step was the application of fluorescent lamps, in which a phosphor converts the ultraviolet radiation originating in the discharge into radiation at a longer wavelength. For the treatment of the skin complaint psoriasis, for example, Philips developed the TL/12 fluorescent lamp, which has a relatively wide emission band centred on 305 nm. After it had been found that the therapeutic effect increased as the wavelength of the radiation approached 315 nm, a new type of lamp was designed — the TL/01. Experiments with this lamp are under way in several Dutch hospitals and in other countries. The colour photograph shows an experimental array of ten of these lamps. They are 1.20 m long, each has a power of 40 W and they have a very narrow emission band with a maximum at 311 nm. The first results from these experiments look very promising.

[*] From Philips Technical Review, January 1938.

Philips Tech. Rev. 44, No. 3, 76-80, July 1988

Bistability in quantum-well lasers

A. I. Kucharska, P. Blood and E. D. Fletcher

Since the early sixties there has been a growing interest in using optical nonlinearities of semiconductor materials for optical logic. Amongst a variety of devices particular attention has been given to the operation of inhomogeneously pumped injection lasers showing two stable light-output levels at the same injection current. Recent advances in the techniques for semiconductor-layer growth have made possible the fabrication of lasers with very thin active layers known as quantum wells. The article below presents some preliminary results of an investigation of the optical bistability in inhomogeneously pumped quantum-well lasers.

Introduction

An inhomogeneously pumped semiconductor injection laser may show optical bistability in the form of two stable light-output levels for the same value of injection current [1]. This nonlinear optical effect relies on saturation of the light absorption in a passive region in the device. It offers the possibility of making optical switching devices to be used for modulating light sources and processing information which is being transmitted or manipulated by means of light beams.

In recent years there has been particular interest in the multiple-quantum-well (MQW) laser, where the light is generated in a set of GaAs layers which are thinner than 20 nm and which are sandwiched between layers of $Al_xGa_{1-x}As$ with a larger band gap [2]. In the active layers the motion of electrons and holes perpendicular to the interfaces is quantized. In addition to fascinating physical phenomena, MQW lasers show some practical advantages such as a relatively low threshold current and a short emission wavelength [3]. It is also expected that the nonlinear optical effect due to inhomogeneous pumping is stronger in MQW lasers than in lasers having a thick active layer of 'bulk' GaAs. The ability to make use of this enhanced nonlinearity could lead to the development of highly efficient electro-optic logic elements.

The fabrication of MQW lasers requires advanced growth techniques such as molecular beam epitaxy (MBE), which has become highly developed at Philips Research Laboratories in Redhill, England [4], or metal-organic vapour-phase epitaxy. MBE is a refined form of vacuum evaporation in which molecular (or atomic) beams from effusion cells impinge upon a heated substrate under ultra-high vacuum conditions. The layer-growth rate for a material like GaAs is

Dr A. I. Kucharska, Dr P. Blood and Dr E. D. Fletcher are with Philips Research Laboratories, Redhill, Surrey, England.

[1] See for example M. J. Adams, A tentative assessment of semiconductor laser optical bistability, Int. J. Electron. **60**, 123-142, 1986.

[2] Quantum-well structures have recently been described in this journal, in a special issue on layered semiconductor structures, Philips Tech. Rev. **43**, 109-165, 1987.
A description of the theoretical aspects of the quantum well will be given by R. Eppenga and F. M. H. Schuurmans, Philips Tech. Rev. **44**, No. 5, Autumn 1988.

[3] K. Woodbridge, P. Blood, E. D. Fletcher and P. J. Hulyer, Short wavelength (visible) GaAs quantum well lasers grown by molecular beam epitaxy, Appl. Phys. Lett. **45**, 16-18, 1984;
P. Blood, E. D. Fletcher and K. Woodbridge, Dependence of threshold current on the number of wells in AlGaAs-GaAs quantum well lasers, Appl. Phys. Lett. **47**, 193-195, 1985.

[4] B. A. Joyce and C. T. Foxon, Molecular beam epitaxy of multilayer structures with GaAs and $Al_xGa_{1-x}As$, Philips Tech. Rev. **43**, 143-153, 1987.

typically about 1 μm/h, i.e. one monolayer per second, so with beam shutters in front of each cell operating within 0.3 s it is possible to grow very thin layers with interfaces that are 'abrupt' within one monolayer.

In the investigation described in this article, we have performed some preliminary experiments on inhomogeneously pumped quantum-well laser structures in the $GaAs/Al_xGa_{1-x}As$ material system grown by MBE, and the measured light-current characteristics do indeed show hysteresis. It has been possible to demonstrate rapid switching between low and high light-output levels. The mechanism of the optical bistability in MQW lasers was assessed by studying the laser-emission spectrum and the optical absorption spectrum of the passive region.

In this article we first give some details of the MBE-grown laser structures. Next we describe their light-current characteristics and switching behaviour. Finally, the physical processes responsible for the observed bistability are discussed.

Device structures

The structure of an inhomogeneously pumped MQW laser device is shown schematically in *fig. 1.* The epitaxial semiconductor structure was grown by K. Woodbridge using a laboratory-built MBE system with computer-controlled effusion-cell temperatures and shutter operations [3]. The structure has a 200 nm thick waveguiding region of $Al_{0.35}Ga_{0.65}As$ barriers and two 2.5 nm thick quantum wells of GaAs. On both sides cladding layers of $Al_{0.60}Ga_{0.40}As$ were grown. Contact layers of heavily doped n-GaAs and p-GaAs were used to obtain good electrical contacts to the metallizations. A stripe laser, 50 μm wide and 300 μm long, was made by P. J. Hulyer using oxide insulation. The laser operated at a wavelength of 777 nm. Inhomogeneous pumping was achieved by dividing the p contact of the device into two regions with a groove etched through the top metallization and top GaAs contact layer in a direction perpendicular to the oxide stripe. It was thus possible to have a pumped region and an unpumped region within the same Fabry-Pérot cavity.

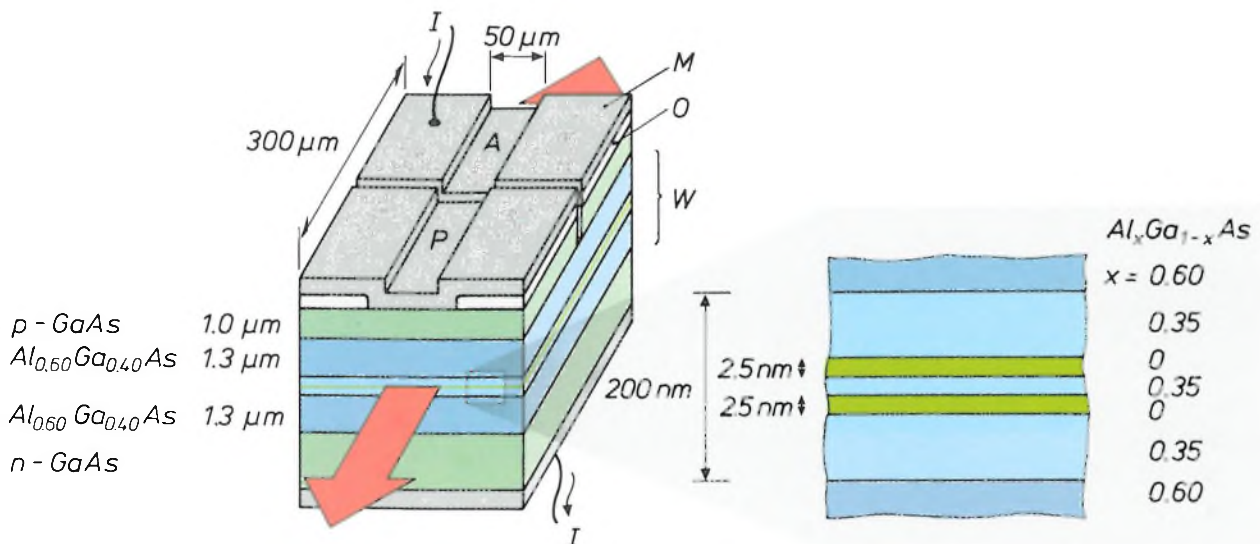

Fig. 1. Schematic diagram of the structure of an inhomogeneously pumped MQW laser device. The device has a length of 300 μm and the current *I* is restricted to a 50 μm wide stripe by insulation with an oxide layer *O*. The laser light *L* is generated in two 2.5 nm thick quantum wells of GaAs sandwiched between layers of $Al_{0.35}Ga_{0.65}As$. The waveguide *W* is formed by two 1.3 μm thick cladding layers of $Al_{0.60}Ga_{0.40}As$. Contact layers of heavily doped n-GaAs and p-GaAs are used for the electrical contact with the metal layers *M*. A groove perpendicular to the stripe has been etched through the top metal layer and top contact layer, resulting in an active region *A* and a passive region *P* for laser operation.

Light-current characteristics and switching

The light-current characteristics were measured in real time by driving one contact segment of the devices with a triangular current pulse, with an overall duration of 800 ns and a repetition rate of 1 kHz, and by detecting the generated light with a fast avalanche photodiode. For the inhomogeneously pumped devices curves with a hysteresis were obtained as shown in *fig. 2* for a typical MQW device. As current is first

injected the light output increases slowly. At higher current the light output increases steeply when the laser operation switches on. If in this state the current is decreased slightly, the laser remains 'on'. When the current is still further decreased the light output suddenly drops to a low level. It is then necessary to drive the device to a higher current in order to turn it 'on' again. The difference between the threshold current for laser action and the turn-off current was not affected by the maximum current, I_{max}, to which the device was driven above threshold. This is also shown in fig. 2 for two different maximum current values, I^a_{max} and I^b_{max}.

The hysteresis observed in the light-current characteristics of these structures suggests that it should be possible to cause them to switch between two stable optical power levels. This was demonstrated by driving the devices with a relatively long pulse ($\approx$ 500 ns) to a current I_1 (fig. 2) within the hysteresis loop, then superimposing shorter ($\approx$ 20 ns) switch-up and switch-down pulses having amplitudes which drove the devices above threshold current and below the turn-off current respectively. *Fig. 3* shows typical oscilloscope traces of the monitored device current and the light output as functions of time. Switching is clearly demonstrated with the light output remaining at a high level after the switch-up pulse was removed and the current returned to I_1. Likewise, the output remained at a low level for the same base current I_1 after the switch-down pulse was applied. Thus at the current I_1, the light output is at one of two stable levels according to the sense of the preceding short switching pulse. The same type of hysteresis and switching was observed for a variety of inhomogeneously pumped MQW devices made from the same slice. The rise time of the light output in response to a switch-up pulse was less than 2 ns, our present experimental limit, and the optical power at the threshold current was a few milliwatts (fig. 2). The hysteresis described here with the associated switching behaviour was not observed for homogeneously pumped structures made from the same materials.

This kind of switching is due to the passive region in the laser cavity, and we have observed similar behaviour in conventional double-heterostructure

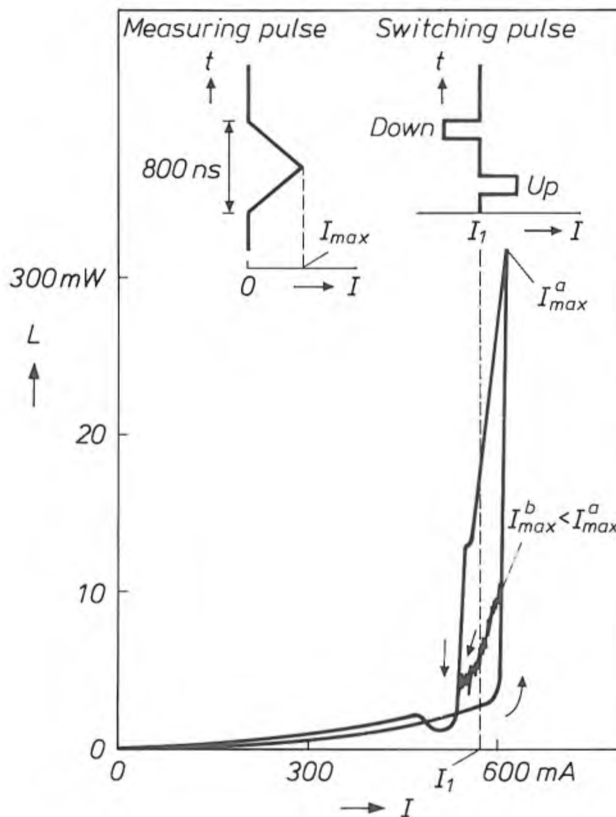

Fig. 2. Light-current characteristic of an inhomogeneously pumped MQW laser device showing hysteresis. Also shown are the forms of the current pulses (current I against time t) used for this measurement and a switching experiment. The device had a total length of 324 μm and the ratio of the pumped and unpumped stripe lengths was approximately 4:1. The current was applied as triangular pulses of 800 ns duration with a maximum value I_{max} above the threshold current for laser action. The turn-off value of the current in the hysteresis loop was not affected by this maximum value (I^a_{max} or I^b_{max}). Because of the hysteresis, two light-output levels exist at the current I_1. As indicated, switching-up and switching-down between these two levels is made possible by applying a short pulse giving a slight increase or decrease of the current with respect to I_1 (see also fig. 3).

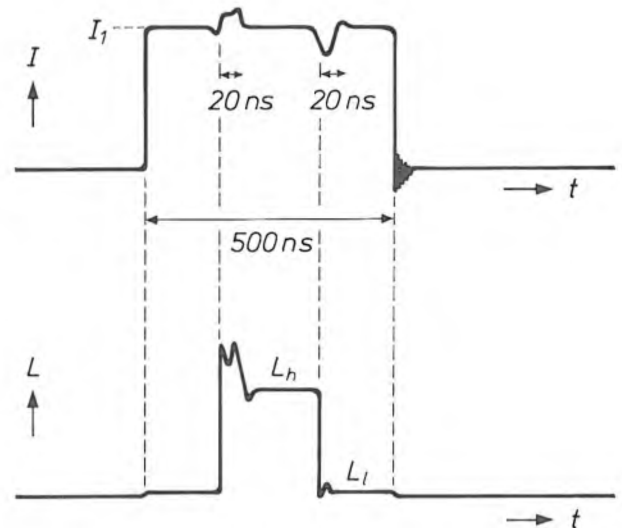

Fig. 3. Current I and light output L against time t showing the switching behaviour of an inhomogeneously pumped MQW laser device. At the current I_1 the light output is either at a high level (L_h) or at a low level (L_l) depending on whether the preceding short (20 ns) switching pulse was upwards or downwards with respect to I_1. The expert help of A. Gowthorpe with the electronics for the pulsed experiments is gratefully acknowledged.

lasers which do not embody quantum wells. We argue below, however, that the mechanism in quantum wells is different from that in bulk materials, and one of the objectives of our research is to determine whether quantum wells offer advantages in these devices.

Mechanism of the bistability

We believe that the observed hysteresis in the light-current characteristics of the inhomogeneously pumped devices is due to reduction of the optical absorption within the unpumped region as the optical power is increased, as in other devices of this type [1] [5]. The importance of the optical absorption can be illustrated by emission spectra measured from each end of an inhomogeneously pumped device at different currents below threshold; see *fig. 4*. Since the light absorption within the cavity is stronger at the short-wavelength side, it has the effect of moving the spontaneous-emission peak to longer wavelengths. In our device, the spontaneous emission is generated only within the pumped region. Consequently, for a single pass through the cavity, this absorption has a more pronounced effect on the spectrum from the unpumped end as no light is generated near this facet. This explains why the spontaneous emission peak from the unpumped end occurs at longer wavelengths than that from the pumped end (fig. 4).

As the current is increased, the gain peak moves to higher energy, thus the emission peak moves to shorter wavelengths. Eventually there is sufficient gain in the pumped region to overcome the absorption losses in the unpumped region over some part of the spectrum. Thus an additional peak appears on the long-wavelength side of the spectrum emitted from the pumped end. This peak coincides with the emission peak from the unpumped end at the threshold current, and represents light which is amplified over several round-trips of the cavity, leading to laser action at threshold.

From the fast rise time of the light output in response to a switch-up pulse we infer that the optical bistability is caused by electronic processes rather than thermal processes. In bulk GaAs, experiment has shown that the effect of an increasing optical power on the absorption depends on the photon energy of the light with respect to the band gap of the semiconductor material [6]. For light having a photon energy lower than the original band gap, the absorption increases due to a reduction of the band gap as a result of Coulomb interactions between the increasing number of charge carriers. For light having a photon energy higher than the original band gap, the absorption decreases with increasing optical power as band filling reduces the probability of valence-to-conduction band transitions because of the Pauli exclusion principle. This effect most probably causes the optical bistability in conventional double-heterostructures with an active layer of bulk GaAs.

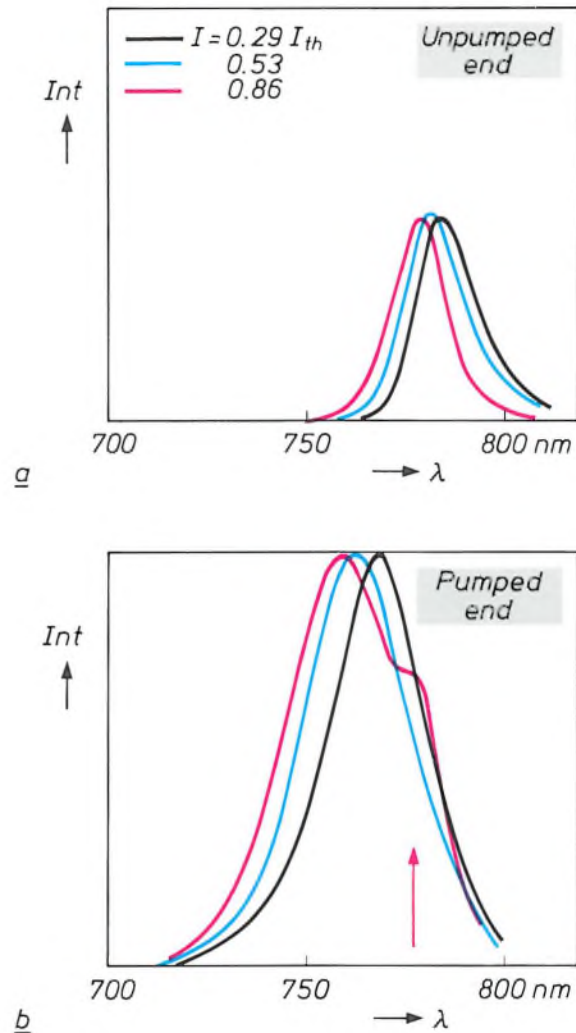

Fig. 4. Normalized emission spectra from the unpumped end and the pumped end of an inhomogeneously pumped MQW laser device. The relative intensity *Int* (in arbitrary units) is plotted against the wavelength λ of the emission for three values of the injection current I below the threshold current (I_{th}) for laser action. The emission peaks for the unpumped end have a lower intensity and are situated at longer wavelengths than those for the pumped end. At increasing injection the maxima shift to shorter wavelength. At $I = 0.86\ I_{th}$ an additional peak appears in the spectrum from the pumped end at about the same wavelength as the maximum for the unpumped end, coinciding with the laser-emission wavelength (arrow) at $I > I_{th}$.

[5] S. Tarucha and H. Okamoto, Voltage-controlled optical bistability associated with two-dimensional exciton in GaAs-AlGaAs multiple quantum well lasers, Appl. Phys. Lett. **49**, 543-545, 1986.

[6] Y. H. Lee, A. Chavez-Pirson, S. W. Koch, H. M. Gibbs, S. H. Park, J. Morhange, A. Jeffery, N. Peyghambarian, L. Banyai, A. C. Gossard and W. Wiegmann, Room-temperature optical nonlinearities in GaAs, Phys. Rev. Lett. **57**, 2446-2449, 1986.

In MQW devices, however, the absorption at the band edge may be strongly affected by the presence of bound electron-hole pairs known as excitons [7]. At low carrier densities excitons appear much more strongly in MQW systems than in bulk material due to the effects of spatial confinement which increase the probability that the motion of an electron and a hole will be correlated to form an exciton, and increase the binding energy of such an electron-hole pair. Thus large resolved exciton peaks are observed in the absorption spectra of MQW structures even at room temperature. The active region of the device used in this work was sufficiently lightly doped (10^{16} cm^{-3}) for excitons to be present in unpumped material. At high carrier densities, however, the excitons are screened out by many-body interactions and the absorption saturates, giving rise to a large optical nonlinearity at these energies.

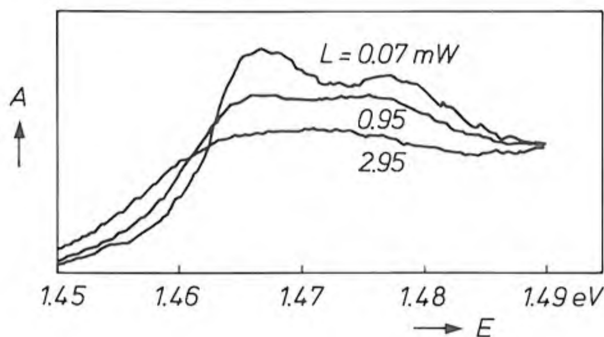

Fig. 5. Room-temperature absorption spectra of an MQW structure having a hundred 8.5-nm quantum wells, measured with the light propagating perpendicular to the wells. The sample was grown by MBE in the same system as the bistable devices. The absorption A, measured at three different levels of the incident optical power L, is plotted in arbitrary units against the photon energy E. Whereas the absorption increases with increasing power at the low-energy side ($\approx$ 1.45 eV), it decreases at the energy where excitonic absorption occurs. The data for this figure were provided by A. Miller, of the Royal Signals and Radar Establishment, Great Malvern, England.

Fig. 5 shows the absorption spectrum of an MQW structure having 8.5 nm thick quantum wells, grown by MBE in the same system as the present bistable device structures, measured for three optical-power levels with the direction of light propagation perpendicular to the wells. It can be seen that the exciton peaks present at low power levels are screened out with increasing optical intensity, while the simultaneous effect of band-gap reduction is to bring the continuum absorption edge to lower energies. Thus the net result is that the absorption increases at low energies, but decreases in the vicinity of the exciton peaks. Above the original band edge the absorption may also decrease due to band filling. In our case, the inhomogeneously pumped MQW devices with 2.5-nm wells operate below the original band edge in the region of the excitonic peaks in the absorption spectrum. Thus the decrease in absorption was provided by the excitons and not by the continuum. The subsidiary peak in the emission spectrum of fig. 4, at which the device switches, thus arises from the decreasing losses at the exciton resonance.

An additional effect which could reduce the absorption below the band edge in inhomogeneously pumped MQW structures is the quantum-confined Stark shift of the band edge under the influence of an electric field. This shift arises from the change in the shape of the potential distribution in a quantum well when an electric field is applied across it. The potential changes in such a way that the energy difference between the lowest quantum states of the electrons and holes is reduced [8]. In the unpumped segment of the bistable MQW laser structure there is a built-in field due to the presence of the p-n junction. This field is reduced at high injection current by carriers generated upon absorption of light from the pumped segment. This reduces the Stark shift, so that the absorption edge moves to a higher energy at a higher injection current. We have observed a shift of the absorption edge of this structure of approximately 3-4 meV for an applied bias of 9 V (6.8×10^5 V/cm) whereas the built-in field is only about 1.8×10^5 V/cm. Even if this field is reduced to zero under optical excitation, the resulting shift is less than about 1 meV, which is too small to be responsible for the bistability we observe.

In conclusion, we believe that the bistability of the inhomogeneously pumped MQW devices is due to excitonic saturation. Experiments are planned to investigate this further and to compare the performance of MQW and bulk materials in these switching devices.

Summary. Hysteresis has been observed in the light-current characteristics of inhomogeneously pumped GaAs-$Al_xGa_{1-x}As$ laser structures which were grown by molecular beam epitaxy and whose active regions consisted of 2.5 nm thick multiple quantum wells (MQW). Fast switching ($<$ 2ns) between low and high light-output levels was demonstrated. The observed bistability was due to saturation of the optical absorption in the passive region of these structures at high injection currents. The MQW laser devices operated in the wavelength region of the excitonic absorption and their bistability was ascribed to the decrease of this absorption at higher light intensities.

[7] D. S. Chemla and D. A. B. Miller, Room-temperature excitonic nonlinear-optical effects in semiconductor quantum-well structures, J. Opt. Soc. Am. B 2, 1155-1173, 1985.

[8] D. A. B. Miller, D. S. Chemla, T. C. Damen, A. C. Gossard, W. Wiegmann, T. H. Wood and C. A. Burrus, Electric field dependence of optical absorption near the band gap of quantum-well structures, Phys. Rev. B 32, 1043-1060, 1985.

Philips Tech. Rev. 44, No. 3, 81-88, July 1988

Chemical modification of surfaces

J. J. Ponjeé and P. N. T. van Velzen

Some of the materials used in the latest products of the electronics industry go through minute but extremely effective surface modifications as a part of the fabrication process.

Outlines of a new technology

In some sectors of technology the surface of the product cannot be allowed to remain in its 'natural' state. The product and the method of producing it must achieve standards of quality that can only be met by adapting the nature of the surface appropriately. The chemical means used for modifying the *adhesion* and *'release'* behaviour of materials by manipulating the chemical structure of the surface will be discussed in this article as an example.

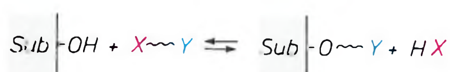

Fig. 1. Diagram illustrating the chemical modification of surfaces. A substrate surface *Sub*, on which reactive groups are present (a hydroxyl group is shown here), is allowed to react with organic molecules possessing two functional groups. One functional group, *X* (red), reacts with a hydroxyl group, the other, *Y* (blue), provides the surface with the required new property.

The modification is made by applying a layer of the order of one molecule in thickness to the surface. In general the molecules of the layer must possess two functional groups, one to react with the functional groups of the 'old surface' and one to determine the required new property of the 'new surface' (*fig. 1*). The bond between these bifunctional molecules and the surface should preferably be covalent, so that the strength of the new entity is not substantially less than the bonding strength in the substrate. The thickness of the applied layer should have an order of magnitude of no more than one molecular layer, because the bulk properties of the new entity should be relatively close to those of the original substrate. The aim is also to keep the morphology and topography of the surface in the original state.

A precondition for this surface modification is that functional or reactive groups (reactive sites) should be present on the surface, and that they should not be 'shielded' by impurities. This means that the surface must be subjected to a special chemical cleaning procedure [1] before the actual chemical reaction.

Another precondition for the method is that the interface between the new layer and the substrate should permit stress relaxation on shrinkage and expansion. The bifunctional molecules used for this are generally organic molecules such as organosilanes, which form bonds at the original surface in the following way:

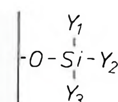

In this structural scheme Y_1, Y_2 and Y_3 represent organic substituents. It is assumed that the -O-Si- or

J. J. Ponjeé is with Philips Research Laboratories, Eindhoven; Dr P. N. T. van Velzen, formerly with these Laboratories, is now with the Philips Industrial & Electro-acoustic Systems Division, Eindhoven.

[1] A good cleaning procedure is described in J. R. Vig, UV/ozone cleaning of surfaces, IEEE **PHP-12**, 365-370, 1976.

siloxane bond here can easily be hydrolysed by water, so that in the presence of ambient moisture the following equilibrium is established:

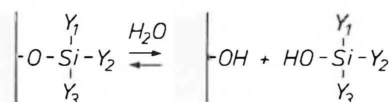

The existence of such an equilibrium (which therefore gives a 'dynamic interface' instead of a rigid network link) would indeed permit the required stress relaxation on shrinkage and expansion.

In the next section we shall first give some examples of the different areas of technology in which this method of chemical surface modification is being successfully used. We conclude that section with a more detailed discussion of one particular area of application: the replication of aspheric lenses, where adhesion and release behaviour are both important.

The application of chemical surface modification obviously requires a thorough knowledge of the surface chemistry. It is necessary to establish whether the reactive sites are indeed present on the surface to be modified, or whether they can be formed there. The degree of surface cleanliness must be known, and the best cleaning procedure. It will also be necessary to know whether the reaction between the reactive groups on the surface and the reagents has in fact been completed in the expected way.

The answers to such questions must be provided by an appropriate analytical method or combination of analytical methods. The following points should be borne in mind when formulating the requirements to be met by such a method.

- Since the chemical modification of the surface is restricted to the outer molecular layer, the number of molecules involved will in general be no more than 10^{13} to 10^{15} per cm^2. This sets the detection limit (or sensitivity) of the analytical method. Many methods are therefore ruled out from the start.
- Since the majority of reagents used are organochemical in nature, a complete picture of the surface chemistry not only requires data on the *composition* of chemical elements at the surface but also calls for information on the molecular *structure* at the surface.
- The analytical method should be sufficiently 'surface-sensitive' for the results relating to the outer molecular layer to be extracted from the information obtained. This is a particular problem when the bulk material and the surface layer have a comparable structure, which is so for modified polymer surfaces, for example.

We conclude the article with a discussion of two analytical methods that meet these requirements: IETS and SSIMS. Results will be given of some analyses performed with these methods for making aspheric lenses by the replication process.

Examples of applications

Improving the adhesion between a 'novolac'-based photoresist and silicon

The photoresists widely used in IC manufacture have the property of becoming more soluble (positive resist) or less soluble (negative resist) on exposure to illumination. In the subsequent 'development' process the exposed parts of the positive resist (or the unexposed parts of the negative resist) should be easily removable. At the same time the parts of the resist that do not have to be removed should adhere so firmly to the silicon surface that is no danger of them becoming detached during the development.

One of the best known photoresists, which we shall take here as an example, is 'novolac', a group of photosensitive materials used in combination with a phenol-formaldehyde resin [2]. We have found that the use of an aminosilane compound, N-[(3-trimethoxysilyl)propyl]ethylene diamine (*fig. 2*), significantly improves the adhesion between this photoresist and silicon. We assume that this involves three chemical effects. A part (shown in red) of the methoxysilyl groups of the aminosilane molecule reacts with hydroxyl or silanol groups at the silicon surface. These silanol groups always form on the silicon surface in the presence of ambient moisture. Some of the alkaline amino groups (shown in blue) enter into an acid-

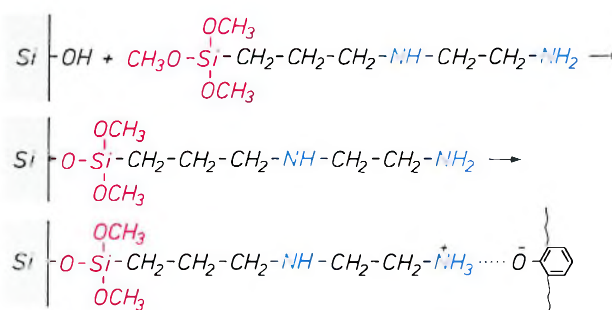

Fig. 2. Reaction equations for the chemical modification of a silicon-oxide surface on which a 'novolac'-based photoresist is to be deposited. The hydroxyl or silanol groups present on the substrate surface form bonds with the aminosilane molecules. The bond is effected by the trimethoxysilyl group of the molecule, shown in red. (The reaction described here relates to a single hydroxyl group with an aminosilane molecule, but two hydroxyl groups may also be involved in this reaction; this also applies to the reactions in figs 3, 4 and 7.) The amino groups, shown blue, are alkaline and can therefore react, in the way shown, with acidic phenolic groups, which are present in the 'novolac' component of certain photoresists.

base reaction with the acidic (mainly phenolic) groups of the novolac. For the resist reaction to occur more than one amino group per silane molecule is required: if only one amino group is present it is highly probable that the interactions of this group with the resin will be inhibited by the silanol groups of the surface, which are also acidic. This effect is sufficiently compensated by the presence of a second amino group.

Improvement of the adhesion between photosensitive polyimide and silicon

In one of the final stages of fabrication integrated circuits are coated with a layer to protect them from α-radiation. A lithographic process is also used in this process step to leave spaces open for the contacts made by the subsequent metallization. A photosensitive polyimide is a suitable material for such a protective layer.

This material is applied in the form of soluble polyamide acids, made insoluble at the appropriate places by illumination through a mask; the complete layer is then converted into a strongly cross-linked polyimide network by curing it at 330 °C [2].

In both the development and curing processes, however, it is difficult to obtain well-defined patterns because there may be a considerable difference in expansion coefficient between the two materials. Another difficulty arising from the difference in expansion coefficient is that the protective coating may come away from the substrate during the curing process. We have achieved good results with the aminosilane compound mentioned above, which takes part in network formation during exposure and curing as indicated schematically in *fig. 3* — i.e. by addition of the amino groups to the unsaturated compound.

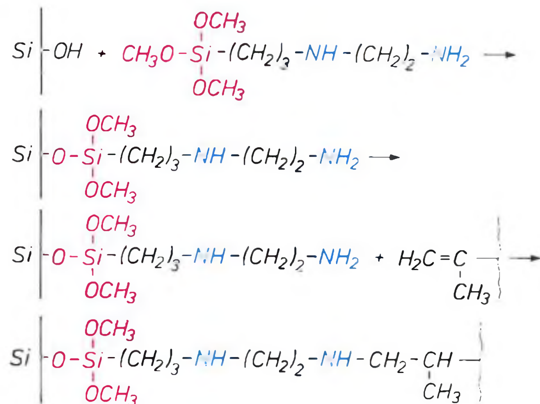

Fig. 3. The same aminosilane compound as in fig. 2, which has reacted in the same way with a silanol group of the silicon substrate, and then forms a bond with a polyamide chain (shown here as a wavy line). In the latter case the bond has been formed between an amino group (shown in blue) in the aminosilane compound and an unsaturated bond in the polyamide chain.

Improving the adhesion between noble metals and glass

Certain substrates such as glass can be given desirable reflection properties by depositing noble metals such as gold, silver and platinum on their surfaces. It will often be necessary to preserve the original shape of the substrate surface as far as possible, especially if it is flat. This gives problems if the noble metals do not adhere to the substrate very readily.

The adhesion can be improved by first allowing the substrate to react with mercaptosilane molecules, which contain SH functional groups (*fig. 4*). The adhesion is improved because the noble metals form bonds with the SH groups. The metal can then be grown on the bonded metal atoms by vacuum evaporation, for example.

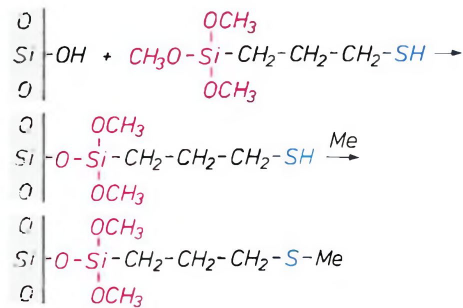

Fig. 4. Noble metals (*Me*) such as gold, silver and platinum can be bonded to glass and other surfaces by a mercaptosilane compound. The metal atoms bonded in this way act as nuclei on which the required metallization layer can be produced in a conventional vapour-deposition process.

Improving the adhesion of the silver mirror coating on video discs

On video discs such as the Philips LaserVision video disc, the silver coating that reflects the laser light must adhere firmly to the substrate material of the disc, which is polymethyl methacrylate (PMMA). This firm adhesion must be achieved without essentially changing the surface pattern of pits that contains the recorded information. These difficult requirements can be met by first applying a monomolecular layer of tannin to the surface, and then depositing tin on the tannin by adsorption from solution.

Just why tannin adheres to the surface of synthetic materials is not as yet entirely clear. It is however known that the tannin forms complexes with Sn(II) ions. These Sn(II) ions adhering to the tannin form silver atoms from silver ions by a redox reaction. The silver atoms deposited then act as nuclei for the 'electroless' deposition of a silver reflecting coating.

[2] L. K. H. van Beek, Polymer chemistry in the electrical industry, Philips Tech. Rev. 42, 149-159, 1986.

Adhesion and release in the replication method of making aspheric lenses

As our last example we shall discuss the application of chemical surface modifications in the fabrication of aspheric moulds and lenses by the replication method.

The procedure followed in this method is first to make a roughly *spherical preform* ('body') in glass and then to apply a thin film of resist to it. The resist would typically be a methacrylate resist, which polymerizes on exposure to ultraviolet light. The resist film is cured in the required *aspheric* shape by pressing it against an aspheric mould and then illuminating it (*fig. 5*). The *aspheric mould* from which the preform is obtained is made with a very-high-precision lathe such as the Colath [3] which machines a relatively soft material like aluminium extremely accurately to produce the required aspheric shape.

In this replication method there are problems of both adhesion and release. We have solved the problem of *release* from the aluminium mould by allowing the aluminium surface to react with a trimethylsilane compound, N,N-diethyl-1,1,1,-trimethylsilylamine, as shown in *fig. 6*. This compound reacts with the hydroxyl groups that always form on an aluminium surface exposed to the atmosphere, and in the process the trimethylsilyl groups form covalent bonds with the surface while the amine is desorbed. This reaction is limited to a single monolayer. In this way the aluminium becomes coated with inert hydrophobic groups that completely inhibit adhesion to the surface and therefore facilitate release.

To improve the *adhesion* of the photopolymerized resist to the preformed spherical bodies in glass, the surface of the glass can be modified in the way shown in *fig. 7*. The functional groups in blue, the methacrylate groups, are of a similar nature to the functional groups that initiate and take part in the network formation on exposure to illumination.

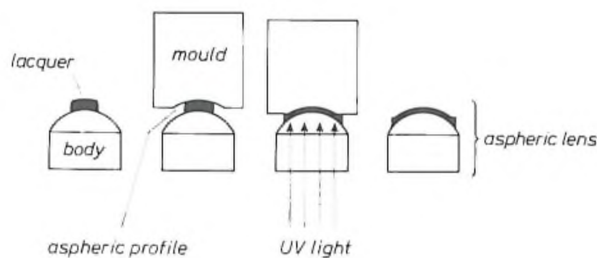

Fig. 5. The principal process steps in the replication method for making aspheric moulds and lenses.

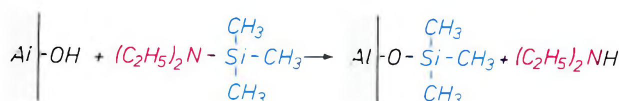

Fig. 6. Reaction scheme for producing a layer with good release properties on an aluminium substrate. The trimethylsilyl groups (in blue), which ultimately constitute the substrate surface, provide no opportunity for adhesion to the surface.

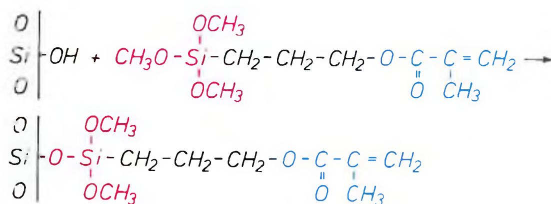

Fig. 7. Reaction equation for a layer to improve the adhesion to a glass substrate. The terminal unsaturated bond (blue) is highly reactive and participates in the network formation that occurs as soon as a photopolymerizing material on this layer is exposed to illumination.

Analysis of chemically modified surfaces

In the introduction we mentioned the special requirements placed on the analytical methods to be used in this work. In view of these requirements we have mainly used inelastic electron-tunnelling spectroscopy (IETS) and static secondary-ion mass spectroscopy (SSIMS) for the applications considered here.

IETS; the method [4]

Inelastic electron-tunnelling spectroscopy is a method that can be used to measure the vibrational spectra of molecules adsorbed on a metal-oxide surface. The method is based on the tunnelling of electrons through an insulator. *Fig. 8* is a diagram of the cross-section of a tunnel diode used in this method.

It is known from quantum mechanics that in a structure like the one in fig. 8 the probability that electrons from metal *3* will be found in metal *4* at a particular time is not zero for very thin insulators but has a finite value — even if the energy of the electrons in that metal is lower than the energy barrier formed by the insulator. The converse is also true; as long as there is no potential difference between *3* and *4*, the net tunnel current is zero. If a voltage is applied, a tunnel current will flow. By analogy with conventional conductors, a tunnel resistance can then be defined that in theory will increase exponentially with the thickness of the insulator. The resultant tunnel current consists of two components (*fig. 9*): an 'elastic' tunnel current (*1*) that gradually increases as a function of the applied voltage (from V = 0), and an 'inelastic' tunnel current (*2*), which also increases gradually, but only from a threshold value E_{min}. This threshold value E_{min} is related to the energy transferred by the electrons to the molecules or the atoms

(or both) of the insulator. The frequency ω of the excitations generated by the electrons can be found from $E_{\min} = eV_{\min} = h\omega/2\pi$, where h is Planck's constant and e the electronic charge.

In reality, of course, a layer of organic molecules on an insulator would not have a single threshold value $E_{\min}$ but several, corresponding in theory to the existing number of molecular vibrations and electronic excitations.

The region we are most interested in is the one corresponding to a potential difference of between 40 and 500 meV, which contains most of the molecular vibrations (with wave numbers between 300 and 4000 cm^{-1}).

Accurate measurement of the current-voltage characteristic of a tunnel diode, as in fig. 8, will thus give the vibrational spectrum of the organic layer

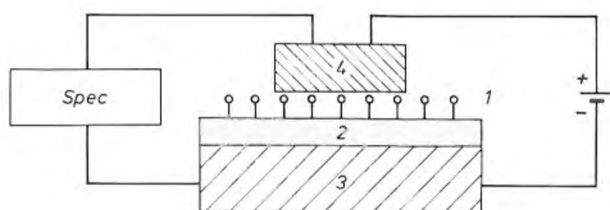

Fig. 8. Diagram of the cross-section of an arrangement for measuring IETS spectra. The organic molecules *1* under investigation are applied to an insulating layer *2* sandwiched between two metal layers (*3* and *4*); the complete device forms a tunnel diode. *Spec* IETS spectrometer. See also fig. 9.

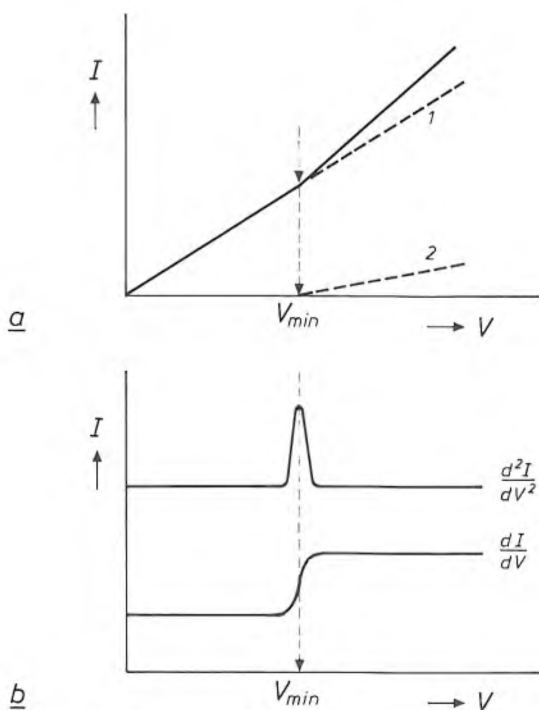

Fig. 9. *a*) The total tunnel current I generated as a function of a voltage V in the arrangement in fig. 8 consists of an 'elastic' component (*1*) and an 'inelastic' component (*2*), occurring after a threshold value $V_{\min}$. *b*) In practice, modulation techniques are used to determine the second derivative d^2V/dI^2 directly as a function of V, which is proportional to d^2I/dV^2.

on the surface of the insulator. It turns out, however, that the change in the tunnel current as a result of 'opening' an inelastic tunnel channel (the increase in the slope at $V_{\min}$ in fig. 9*a*) remains well below 1%, and is almost undetectable. These threshold values can nevertheless be determined as peaks at the potential difference $V_{\min}$ by measuring the tunnel current as a function of the second derivative of the potential difference, as illustrated schematically in fig. 9*b*.

At this point we should say something about the potential of the IETS method — and its limitations.

- The detection sensitivity of IETS is far below one monomolecular layer.
- IETS measurements are made at 4.2 K or below to reduce thermal line-broadening. The top metal (*4*) generally used is lead, which is a superconductor at this temperature, thus slightly improving the resolution. In practice, linewidths of 15-25 cm^{-1} are achieved, and this is amply sufficient to discriminate between the relevant peaks, even for complex organic molecules. While lead has the advantage that it is a superconductor at 4.2 K, it can also be evaporated under relatively mild conditions, and it is a metal that is fairly inert to organic compounds.
- A limitation of the IETS technique is that it can only be used on metals on which a very thin (about 2 nm) and electrically stable insulator can be formed reproducibly. Because of the very strict conditions that apply to the breakdown voltage of the insulating material ($> 2.5 \times 10^6$ Vcm^{-1}), tunnel spectroscopy has so far been limited to aluminium, magnesium, tin and lead. Most experiments have been performed on aluminium-oxide surfaces.

IETS; analysis results

As an example of the application of IETS for the analysis of chemical surface modification in practical situations, we shall discuss the modification of aspheric aluminium moulds (which have been oxidized at the surface) with N,N-diethyl-1,1,1,-trimethylsilylamine. Because the quality of the insulating oxide layer for IETS measurements must be extremely high it is impossible to perform measurements directly on the mould. The measurements are therefore carried out on aluminium substrates vapour-deposited on glass.

Fig. 10a gives the IETS spectrum of an uncoated surface of aluminium oxide. Only two bands are really distinct and easily assigned; these are the band at 940 cm^{-1}, due to an Al-O 'stretching' vibration, and

[3] T. G. Gijsbers, COLATH, a numerically controlled lathe for very high precision, Philips Tech. Rev. 39, 229-244, 1980.
[4] P. K. Hansma, J. Electron Spectrosc. & Relat. Phenom. 30, 163-174, 1983.

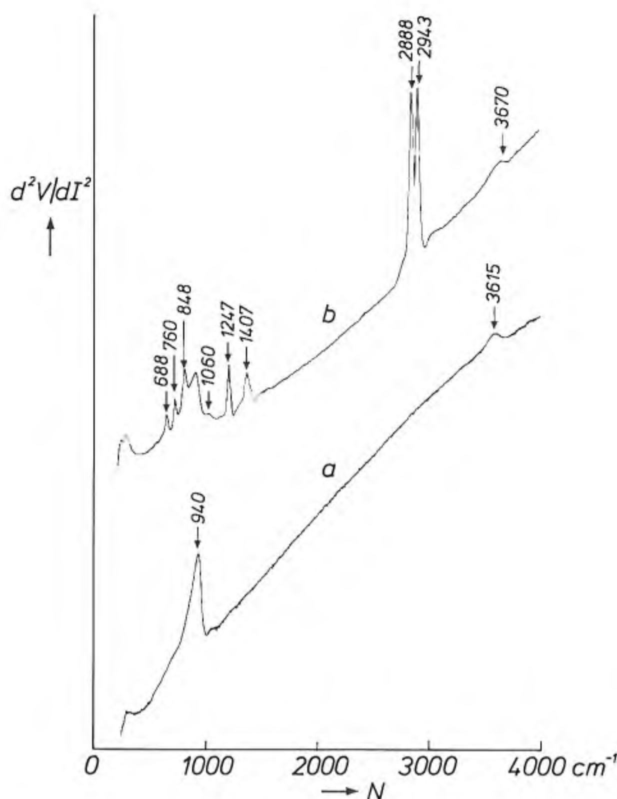

Fig. 10. IETS spectra of (*a*) a clean aluminium-oxide surface and (*b*) the same surface after reacting with N,N-diethyltrimethylsilylamine. The values determined for d^2V/dI^2 are given in arbitrary units as a function of the wave number $N(=\omega/2\pi c)$, where c is the velocity of light. See the text for the identification of the peaks in the spectra, and fig. 6 for the reaction equation.

the band at about 3615 cm^{-1}, due to the O-H stretching vibration of hydroxyl groups at the surface. The initial requirements for the chemical surface modification, as expressed above — a clean surface with reactive sites, in this case the aluminium-hydroxide groups — have therefore been met.

After this surface was brought into contact with the vapour of the aminosilane mentioned above, the IETS spectrum of the resultant aluminium-oxide surface was measured (fig. 10*b*). It is clear that the new surface no longer consists of clean aluminium oxide. The complete spectrum can be interpreted with the aid of infrared and Raman data for vibration frequencies of functional groups in organic molecules. This will not be discussed here in detail [5].

The main conclusions that can be drawn from the measurements on this system are mentioned below. Most of the bands in fig. 10*b* can be directly assigned to the $Si(CH_3)_3$ group, and no indications can be found in the spectrum for the presence of a functional $N(C_2H_5)_2$ group. The bonding of these $Si(CH_3)_3$ groups to the aluminium oxide can also be derived from a band (of low intensity) at 1060 cm^{-1}; this band can be assigned to the asymmetric Al-O-Si stretching vibration in the Al-O-$Si(CH_3)_3$ structure. It follows that the model for this surface reaction presented in fig. 6 is in good agreement with the results obtained with IETS.

The shape of the spectrum and the intensities of the bands do not depend on the length of time the oxide is exposed to the aminosilane vapour, which indicates that the reaction is fast and also, in complete agreement with the model, is limited to the formation of one monomolecular layer. Although in ordinary conditions the Al-O-Si bond can easily be broken in the presence of water (see the introduction), under these conditions it takes more effort to remove the $Si(CH_3)_3$ groups from the surface with water. This is because the new surface is made hydrophobic by covering it with these groups, and cannot therefore be wetted easily. The surface layer thus obtained therefore possesses excellent release properties. Although these measurements were performed on a model system, there is no reason to assume that a thoroughly cleaned aluminium mould (on which a clean oxide is present) cannot be modified in an identical manner.

SIMS; the method [6]

The outer molecular layer of a material can be analysed with SIMS. The surface of the material is bombarded with energetic particles (energy 1-20 kV), generally ions but atoms are sometimes used, and the bombardment releases secondary particles from the surface. This is the process known as sputtering. A small proportion of the sputtered particles are secondary ions — both positive and negative — which can be detected by the principles of mass spectrometry. Depending on the energy and current density of the primary ion beam, there are two limiting cases:

Dynamic SIMS. In this case relatively high beam-current densities are used. The molecular or atomic layers of the material are sputtered at a high velocity mainly as elemental ions. Dynamic SIMS is particularly suitable for determining the *elemental composition* of surfaces (e.g. the depth profile of the doping in semiconductor material); the method cannot generally provide information about the chemical *structure* of the molecules at the surface.

Static SIMS. When low-energy primary ions are used at a low current density (six orders of magnitude less than in the dynamic case) during sputtering, cluster ions of higher mass originating from the outermost monolayers are observed. The structure of ions of this kind provides information about the chemical struc-

[5] P. N. T. van Velzen and M. C. Raas, Surf. Sci. **161**, L 605-L 613, 1985.
[6] A. Brown and J. C. Vickerman, Surf. & Interface Anal. **6**, 1-14, 1984.

ture of the surface (see the introduction). Under these 'static' conditions the total amount of material is small, so that the mass spectrum of the outermost layers of the surface can be measured quasi-non-destructively. This implies that only a negligible fraction of the surface is damaged during the entire measurement (usually about 10^{-3} of a monolayer or less), while the probability that a point on the surface is struck more than once by a primary ion is very small. For the measurement, however, this requires highly sensitive mass-spectroscopic detection of the secondary ions. This is achieved by means of time-of-flight analysis of the secondary ions. This explains the name of the method: time of flight SIMS, or TOF-SIMS; see *fig. 11*.

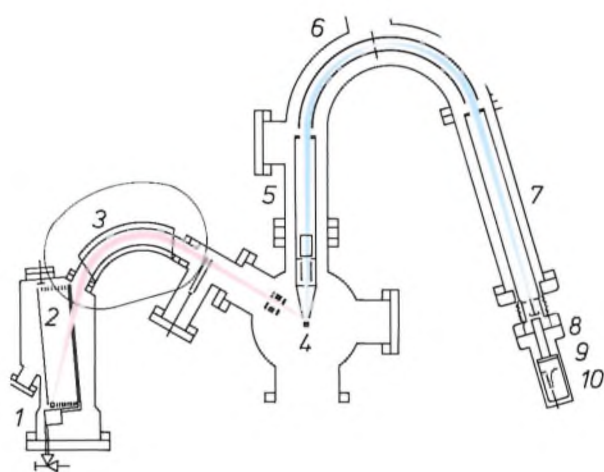

Fig. 11. Diagram of the TOF-SIMS spectrometer used for measuring the SIMS spectra given here. It is located in Prof. A. Benninghoven's Surface Physics group at the University of Münster, West Germany. The instrument consists of a primary ion source (*1*), a deflection plate (*2*), a magnet for mass discrimination and focusing the primary ion beam (*3*), a multiple-focus time-of-flight analyser (*5*, *6*, *7*) and a detector (*8* to *10*). In this instrument a pulsed mass-discriminated primary ion beam is generated (pulse width 10 ns) with an accurately defined energy and a very low mean current (of the order of 1 pA), which sputters secondary ions from the specimen (*4*). These ions are extracted from the surface and accelerated by a pulsed voltage on the entrance plate of the linear drift space (*5*). Mass discrimination of the secondary ions is obtained because of the differences in time of flight through the combination of two linear drift spaces (*5*, *7*) and an electrostatic sector field (*6*); the time of flight is proportional to $\sqrt{m}$, where m is the mass of the ions.

The ions are detected by a single channel plate (*8*), and a scintillator (*9*) optically linked to a photomultiplier (*10*). The detector operates in the single-ion counting mode.

As compared with other methods of secondary-ion mass spectroscopy in the static limit range (e.g. quadrupole-static SIMS), TOF-SIMS has the following very important features:

1. High transmission of the mass-discriminating system (> 10%).
2. Quasi-simultaneous measurement of all the ions of the same sign (the entire mass range is measured for each primary-ion pulse).
3. Good mass discrimination ($m/\Delta m \approx 1000$, where m is the mass and Δm the peak width at half height).
4. Because of 1 and 2 the sensitivity of the spectrometer is very high. A detection limit of 10^{-6} monolayer or better has been demonstrated for a number of systems.
5. The typical measurement time per spectrum is less than 1 minute.

SIMS; analysis results

We conclude with some results of analyses relating to improvement in the adhesion of a methacrylate resist on lanthanum-containing glass, as used in the replication process.

The glass is cleaned with an alkaline soap, rinsed with water and then dried in isopropanol vapour. The modification is performed by exposing the surface to the vapour of 3-methacryloxypropyltrimethoxysilane; it is assumed that a reaction as shown in fig. 7 takes place during this exposure. *Figs 12 and 13* give the

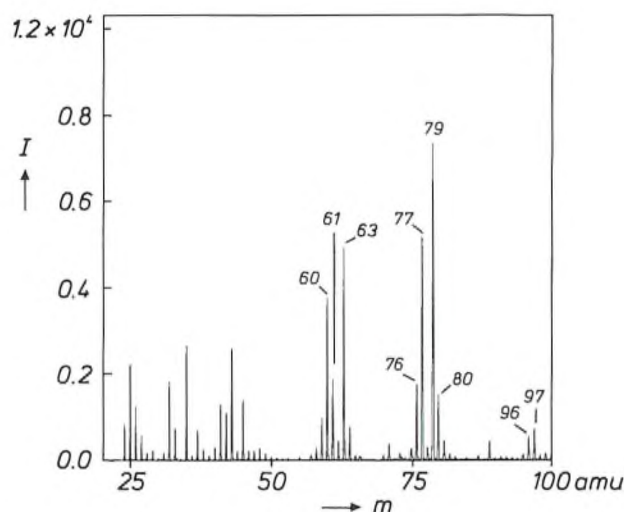

Fig. 12. Negative SIMS spectrum of a cleaned surface of lanthanum-containing glass. Owing to adsorbed residues of alkaline soaps used in cleaning, the spectrum contains peaks attributable to SO_4^-, $H_2PO_4^-$, PO_3^-, SO_3^- and PO_2^- (at 96, 97, 79, 80 and 63 amu). The large peaks at 60, 61, 76 and 77 amu (for example) correspond to SiO_2^-, SiO_2H^-, SiO_3^- and SiO_3H^- respectively.

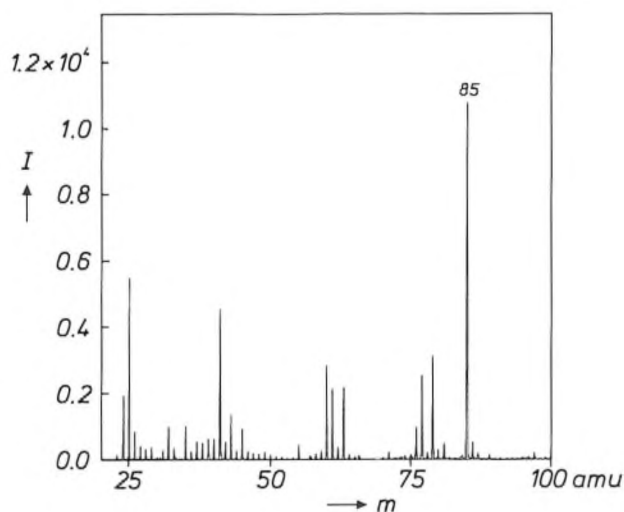

Fig. 13. Negative SIMS spectrum of the same surface as in fig. 12, after it has been allowed to react with a methacryloxysilane. Fig. 7 gives the assumed chemical structure of the modified surface. The largest peak in the spectrum is now observed at 85 amu, and is assigned to the methacrylate anion, $CH_2 = C(CH_3)COO^-$.

negative SIMS spectra of the cleaned and modified glass surface, respectively. Some details of the spectra will now be discussed.

The spectrum of fig. 12 shows that even after cleaning the glass surface is not completely clean. For example, peaks are visible at 96, 97, 79, 80 and 63 amu [7], which must be assigned to SO_4^-, $H_2PO_4^-$, PO_3^- SO_3^- and PO_2^- respectively. These ions originate during the sputtering process from the molecules of residues of the alkaline soaps used for cleaning. The quantities of these soap residues are small, however, as can be seen from a comparison of the intensities of these peaks with those of the intense peaks that originate from the glass substrate, e.g. at 60, 61, 76, 77 amu, and are assigned to SiO_2^-, SiO_2H^-, SiO_3^- and SiO_3H^-.

The same conclusion may be drawn from the positive SIMS spectra of the glass, not shown here, in which the metal ions (including Na^+ and La^+) in the glass can also be observed, demonstrating that these are also present at the surface.

Fig. 13 shows that exposure of the cleaned glass to the vapour of the 3-methacryloxypropyltrimethoxysilane does in fact modify the chemical structure of the surface. The largest peak in the negative SIMS spectrum in this mass range is observed at 85 amu, and originates from the methacrylate anion $CH_2 = C(CH_3)OO^-$, formed by fragmentation of the functional end-group of the methacryloxysilane mentioned above. The reaction with the methacryloxysilane therefore does take place in the way that appears to be necessary for a substantial improvement in the adhesion.

[7] (Unified) atomic mass unit.

Summary. Bifunctional organic molecules that form bonds with a surface with one functional group give new properties to the surface with the other functional group. Adhesion to a surface or release from a surface can be improved by using this method. Preconditions for such chemical surface modification are the presence of reactive sites at the surface, the absence (because of good cleaning procedures) of impurities at these sites, and the possibility of stress relaxation on expansion and shrinkage. Subjects discussed include improvement of the adhesion between a photosensitive resist based on 'novolac' and silicon with an aminosilane, improved adhesion between noble metals and glass with a mercaptosilane, improved adhesion of silver reflecting coatings on LaserVision discs with tannin, an improvement of both adhesion and release in the replication method used for making aspheric lenses, using a methacryloxysilane and a trialkylsilane. The chemical surface modifications described here for the replication method have been investigated by IETS and TOF-SIMS. The principles of these methods are discussed and some results are presented.

Striations in a gas discharge

F. C. van den Heuvel

Optical instabilities in gas discharges have been known almost as long as gas discharges themselves. Fortunately, in most applications their occurrence can be avoided, often by taking external measures adapted to a particular situation. However, a universal remedy requires a better understanding of these effects.

Introduction

In the first half of the 19th century it was discovered that a gas between two electrodes in a sealed glass tube can conduct an electric current. It was also found that the gas emitted radiation. This can be considered as the start of the application of these 'gas discharges' for artificial lighting, since the emitted radiation can have a wavelength in the visible range, or fluorescence from materials on the glass wall can convert the radiation into visible light. In the earliest days strange optical effects were occasionally observed: a pattern of alternate bright and dark regions appeared along the axis of the gaseous column (see *fig. 1*). These discharges are said to contain 'striations', or are described as being 'striated', terms taken from the Latin word 'striae', meaning 'stripes'.

In modern artificial lighting low-pressure mercury/inert-gas discharge lamps (TL, PL and SL lamps) play a leading part. In the design of these lamps efforts are made to create conditions in which the optical effects mentioned above either do not occur or cannot be observed with the naked eye. An artificial light source is obviously required to emit its radiation as uniformly as possible. The parameters that affect the formation of striations in the gas discharge — the composition and pressure of the gas mixture, the dimensions of the tube, the discharge current and the mercury vapour pressure — should be controlled so as to prevent the occurrence of striations, without causing any direct conflict with other characteristics required of the lamp. It is important, for example, that the lamp converts electrical energy into light efficiently, has a long life and is compact. For standard interior lighting it is usually fairly

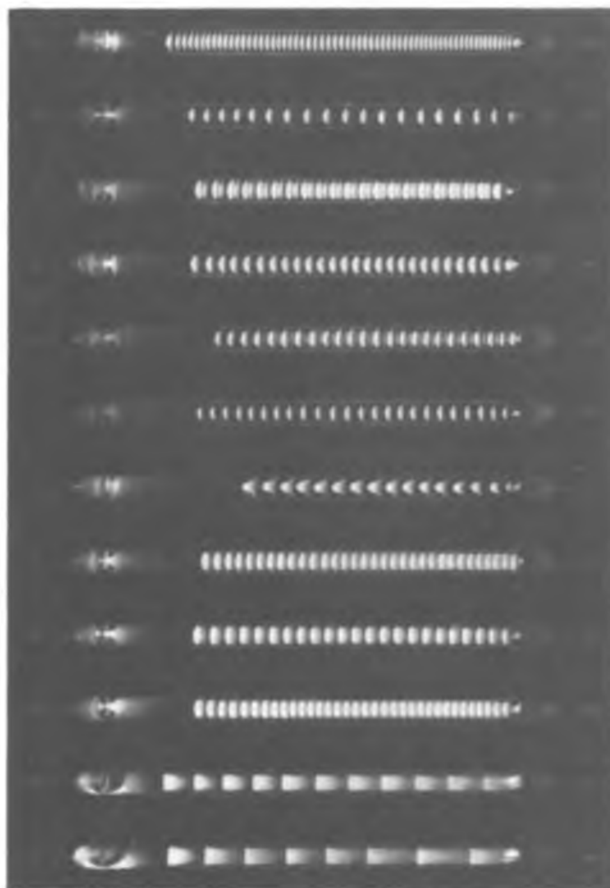

Fig. 1. Some examples of striations in gas discharges. This photograph dates from the early days of gas discharges [1] (1878!). The striations that can be seen in the fourth discharge from below are the ones that most closely resemble an 'instantaneous exposure' of the striations seen in our mercury/argon discharges.

[1] This photograph has been taken from: S. C. Brown, A short history of gaseous electronics, in: M. N. Hirsch and H. J. Oskam (eds), Gaseous electronics, Vol. 1, Electrical discharges, Academic Press, New York 1978, pp. 1-18.

Dr F. C. van den Heuvel is with Philips Research Laboratories, Eindhoven.

easy to find a compromise, because the (r.m.s.) discharge current and the operating temperature, which determine the mercury vapour pressure in the tube, are not subject to marked changes. Even if a compromise should prove difficult it is often still possible to prevent the appearance of striations by taking appropriate external measures. For example, the striations in a fluorescent lamp that fails to reach the required operating temperature because the ambient temperature is too low can be avoided by enclosing the lamp in a suitably modified fitting. Such an approach will not work, however, when a lamp is required to operate without striations in varying conditions. This is the case, for instance, with the integrated lighting systems nowadays installed in large buildings because they are economical of energy. In these systems the lighting level is controlled from a central point to complement the amount of daylight entering the building. There is then a danger that the discharge current through the lamps will become so low that striations appear. The effect becomes worse because a low discharge current gives a lower operating temperature and hence a lower mercury vapour pressure. New precautions then have to be taken to prevent this from happening.

This article is concerned with the way in which the electrical circuit to which the gas discharge is connected affects the occurrence of striations. The discussion will be confined to a d.c. discharge with the current kept just below the critical value at which striations appear. Before considering our experiments and the results, let us first briefly look at the gaseous discharge, the occurrence of striations and an explanation of how they come about. Later in the article there is a discussion of our observations of striated discharges and their relation to the electrical circuit. It will be shown that the striations excite an oscillation in the electrical circuit, and that this oscillation maintains them.

Striations in gas discharges

Fig. 2 gives a diagram of the spatial distribution of an unstriated gas discharge. The distribution is based on the intensity of the generated radiation. Most of the discharge between the two electrodes is taken up by the positive column, which is primarily responsible for the radiation output from the discharge. The phenomena we are concerned with, the striations, appear in this column.

The concentrations of electrons and ions in the positive column are practically identical: macroscopically, the plasma is electrically neutral. The temperature of the electron gas, which is a measure of the velocity of the electrons, is relatively high (about 12 000 K), whereas the temperature of the ion gas is only a few hundred K. The highly mobile electrons with a drift velocity of about 10^4 m/s are responsible for the electric current. The contribution from the much slower ions is negligible. This difference in drift velocity of electrons and ions might have the effect of endangering the neutrality of the plasma, for if the concentration of electrons (and hence ions) is higher in a particular zone of the discharge, the electrons will disappear from this region faster than the ions. This situation is not reached, however. With a separation of even as little as 10 μm between the ion and electron distributions such a strong opposing field is formed that any further drifting apart is prevented. In this way the plasma opposes any large-scale build-up of space charge [2]. This type of field is known as 'ambipolar'. It reduces the applied axial field where the electron density is relatively high and increases it where the electron density is low. This happens in such a way that there is no spatial variation in the electric current: div $j = 0$.

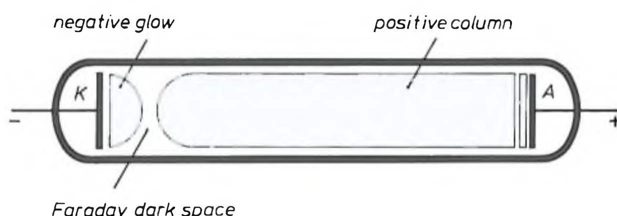

Fig. 2. Spatial distribution of a gas discharge on the basis of the variation in the intensity of the emitted light. Only the most important parts of the discharge are indicated. *K* cathode, *A* anode.

Under certain conditions striations can occur in a gas discharge. Although the effect was known in the early days of gas discharges, no explanation for it appeared till about thirty years ago, when L. Pekarek [3] put forward the following argument. Suppose that, for one reason or another, an unstriated positive column contains a region of some magnitude ($\gg 10\,\mu m$) where the ion density (and hence the electron density) is higher than in the rest of the column. Electrons drifting through this region are then subject to a reduced field because of the presence of the opposing field described above. The electron gas therefore becomes cooler, so that fewer ions are produced by ionization. Since the cooling and heating of the electron gas by an electric field are not instantaneous, of course, the region with the lower temperature will be displaced with respect to the region with the higher density. It will take about 1 μs before the field starts to affect the temperature. In that time the drifting electron gas will

have covered a distance of no less than a centimetre. A local increase in the ion density therefore gives a corresponding decrease in ion density in the adjoining region, and in turn this leads in due course to an increase in the next region, and so on. In the plasma the local temperature profile and the diffusion determine the dynamics of the ion and electron density profiles. Assuming a uniform positive column with a local change in the ion and electron density, Pekarek showed that the assumed local density distribution gives rise to the formation of a kind of 'wave packet'. This propagates along the axis of the discharge, expanding at the same time. The process becomes visible because the intensity of the radiation field changes, as a result of the changed electron temperature. This was how Pekarek explained the origin of moving bright and dark regions in a striated gas discharge.

Depending on the conditions in the plasma, one of the following situations may now arise. If the amplitude of the waves in the packet decreases and the plasma returns to a situation with no perturbations, the plasma is then by definition stable. However, the conditions in the plasma may be such that the amplitude of the waves increases. If the packet then moves more slowly than it expands, the plasma becomes completely unstable. In such a case the plasma does not return to the state of equilibrium. Between these two extremes the plasma is convectively unstable. The term 'convectively' means that the amplitude of the perturbation increases and that its displacement is faster than the spatial growth. The plasma is locally unstable while the packet is passing by, but afterwards a local equilibrium sets in again. We have studied the occurrence of striations in a convectively unstable plasma of this type.

The effect of the electrical circuit on the striations

Fig. 3 shows the circuit used for the experiments. The operating temperature is kept artificially constant by surrounding the discharge tube with a second glass tube and circulating water at a constant temperature of 50 °C in the space between them. The part of the circuit that supplies the direct current for the discharge is decoupled from the load circuit — an a.c. circuit that contains a variable resistance — by an inductance and a capacitance. These have values such that their influence on the load is negligible. The effect of the resistance on the occurrence of striations in the discharge was investigated. The current through the discharge was set just below the critical value; this made the plasma convectively unstable.

The 'wave-packet' perturbations described by Pekarek were indeed observed. They arise as a consequence of noise in the neighbourhood of the cathode and travel towards the anode at a velocity (group velocity) of about 60 m/s. The intensity of the complete wave packet increases as it moves away from the cathode. The phase velocity of the waves 'contained' in a packet has the opposite direction.

The electrical circuit has a definite influence on the effects in the discharge, as can be seen in *fig. 4*. As the external resistance is reduced, the amplitude and the spatial magnitude of the packets increase. When the resistance is sufficiently reduced, wave packets overlap to such an extent that they cannot be distinguished separately and combine to form a travelling wave with a more or less constant wavelength and frequency. It seems as if the wave travels in the opposite direction to the wave packets, but this is only because the phase velocity is positive towards the cathode.

The amplitude of the wave was measured with a moveable photodiode as a function of the distance to the cathode; see *fig. 5*. The photodiode signal consists of two contributions: a signal that would also be measured in an unstriated gas discharge (with the same value everywhere along the column) and a small variation due to the occurrence of striations. The figure only shows the contribution due to the striations. At every position only the maximum value of the variations in the light intensity was recorded. The

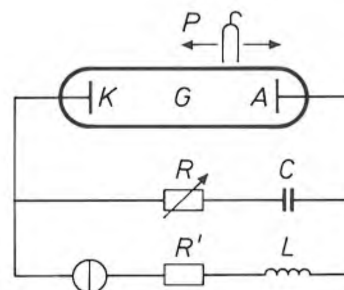

Fig. 3. The experimental arrangement. The discharge tube contains a mixture of argon and saturated mercury vapour at a total pressure of 400 Pa. The tube is 0.6 m long and has an inside diameter of 12 mm. The distance between the electrodes is 0.4 m. The gas discharge G is incorporated in an electrical circuit. The effect of the variable resistance R on the phenomena in the discharge was investigated by measuring the intensity of the emitted radiation with a photodiode P. The capacitance C and the inductance L are included in the circuit to decouple the direct-current and alternating-current parts of the circuit.

[2] The field reaches equilibrium very quickly. At a drift velocity of 10^4 m/s a charge separation of 10 μm is reached after only 1 ns. The charge separation in the plasma is comparable with a dielectric between two capacitor plates. A charge separation on a microscopic scale leads to a macroscopic field, with the dielectric as a whole remaining electrically neutral.

[3] L. Pekarek, The development of a pulse-disturbance in a dc-plasma, Proc. 6th Int. Conf. Phen. Ion. Gases, P. Hubert and E. Cremieu-Alcan (eds), Vol. 2, Paris, 1963, p. 133.

Fig. 4. Variation in the intensity of the emitted radiation, ΔI, as a function of time, measured at a position close to the anode for four values of the variable resistance R. *a*) R = 6 kΩ, *b*) R = 3.7 kΩ, *c*) R = 1.9 kΩ, *d*) R = 0.2 kΩ. The size and amplitude of the wave packets increase as the resistance decreases, until finally a travelling wave is formed. Similar pictures taken at the cathode are qualitatively identical, the only difference being that the size and the intensity of the wave packets are respectively smaller and lower.

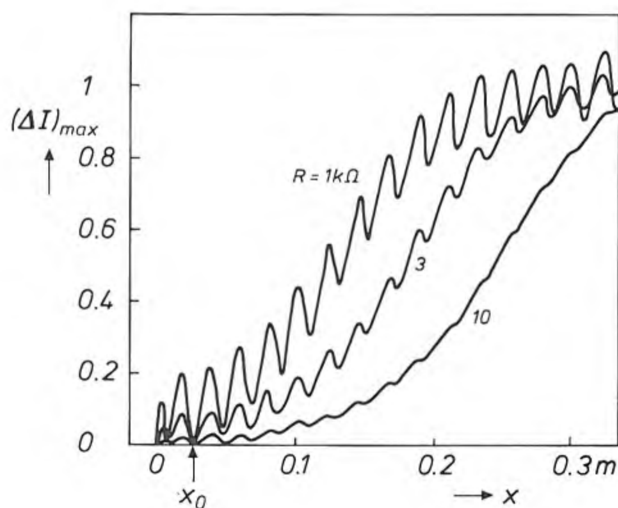

Fig. 5. The maximum value $(\Delta I)_{max}$ of ΔI (the variation in the radiation intensity) due to the occurrence of striations, measured with the photodiode, as a function of the distance x to the cathode. The constant contribution to the photodiode signal has been omitted. At the position x_0 the value of $(\Delta I)_{max}$ is always zero.

actual travelling wave is therefore not shown in the figure, but the variation in the amplitude of this wave as a function of the distance to the cathode. Apart from the sinusoidal modulation — which will be discussed later — it can be seen that the spatial amplitude of the wave increases exponentially with the distance from the cathode, as does the intensity of the individual wave packets. At the anode the wave amplitude reaches a saturation value. When R is decreased the intensity and stability of the wave increase, and the saturation value is reached before the anode. Closer inspection of the curves shows that the exponential growth is identical for the three curves. The rate at which the spatial amplitude of the wave increases is not affected by the resistance and is therefore a property of the plasma. The sinusoidal modulation of the wave amplitude is constant along the column and, like the intensity of the wave, it increases with decreasing R. Fig. 5 also shows that the total wave am-

plitude is zero a few centimetres away from the cathode. We shall return to this point presently.

The most important finding is that the electrical circuit has the effect that the convectively unstable plasma no longer returns to the unstriated situation, which means that the travelling wave is obviously in a state of continuous self-excitation. Because the electrical circuit is known to have an effect on the wave phenomena, the obvious course is to treat the discharge and the circuit as a single entity. The wave is maintained by feedback via the circuit. This situation is rather like that of a noise amplifier that has sufficient feedback to bring it into saturation so that it becomes a self-stabilizing oscillator. The essential difference, however, is in the way in which the coupling between the striation effects in the tube and the circuit is obtained. In the circuit, information can only be transferred in the form of electric currents. The occurrence of a stabilized travelling wave in the discharge means that an alternating current at the same frequency as that of the striation wave must flow in the circuit.

In the next section it will be shown, from analyses of the photodiode signal and the current in the external resistance, that this qualitative assumption can be quantitatively justified.

The oscillation in the circuit

The existence of the oscillation, which is assumed to be responsible for initiating and maintaining the travelling wave in the discharge, can be demonstrated in a number of ways. First of all it will be shown that characteristics of striations can be found both in the photodiode signal and in the electric current. An explanation for this will then be derived from a mathematical description of the wave phenomena.

Measurements

The observations described in the previous section lead to the assumption that the perturbations in the discharge maintain themselves by feedback in the electrical circuit. To test the validity of this assumption, we made a closer analysis of the signals passing through the discharge and through the electrical circuit. A spectrum analyser was used to record the frequency content of the photodiode signal; see *fig. 6.* These spectra were taken for a gas discharge whose discharge current was a little closer to the critical current than in fig. 5. This implies that growing and overlapping wave packets only barely reach the saturated amplitude at the anode (small R) or do not reach it at all (large R). When the resistance is high ($R = 4$ kΩ) the diode signal is irregular, with a noise-gain band around 2.7 kHz. When the feedback is increased (by reducing the resistance) this band remains visible, but increasingly sharper resonance peaks also appear. This picture resembles the frequency spectrum of a laser. Spectra taken of the voltage across the discharge or — and this amounts to the same thing — of the

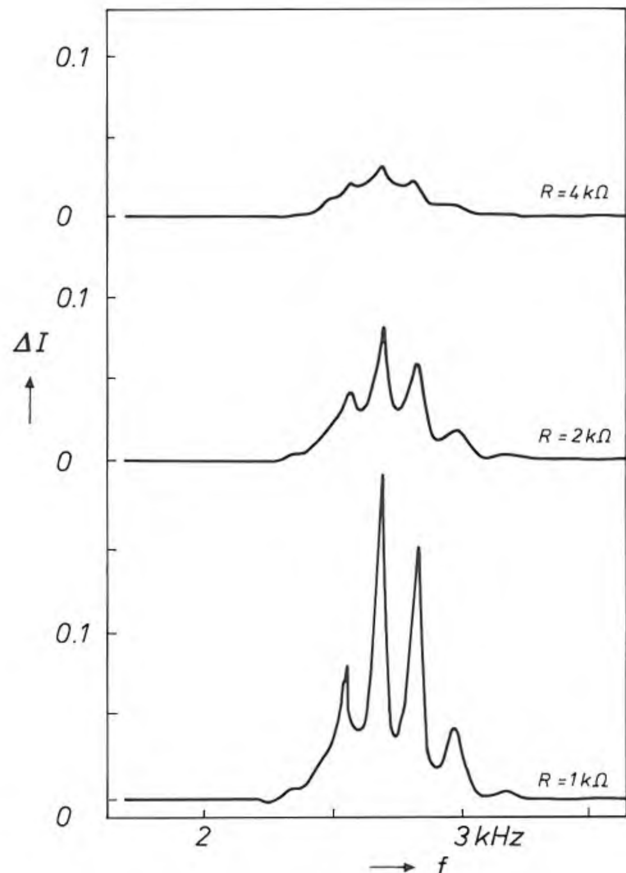

Fig. 6. Frequency spectrum of the photodiode signal for three values of the resistance R. At smaller values of R resonances occur.

current in the feedback resistance, show the same picture; the maxima are at the same frequencies, as can be seen in *fig. 7.*

So the alternating currents assumed do indeed occur, although they are very small — a few tens of μA as compared with the direct current of 100 mA. It appears that the striated discharge acts as a kind of alternating voltage source. In Pekarek's model of a striated discharge, striation waves are accompanied by a local field $E(x,t)$ that ensures the continuity of the current (div $j = 0$). The electric field also takes the form of a travelling wave with an exponentially increasing amplitude. It therefore seems reasonable to extend the model to a voltage source, since the potential *difference* between anode and cathode is equal to

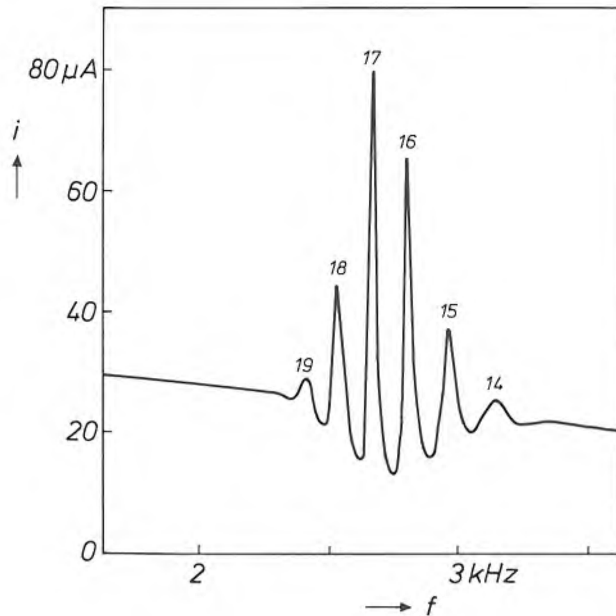

Fig. 7. Frequency spectrum of the alternating current i in the resistance. The background level of about 25 µA is the normal noise level, which is also found in the unstriated discharge. The numbers above the peaks show the length of the positive column in wavelengths at this frequency.

the field $E(x,t)$ spatially integrated from cathode to anode:

$$V(t) = \int_0^l E(x,t)\mathrm{d}x \qquad (1)$$

(with the cathode at $x = 0$ and the anode at $x = l$). It is an alternating voltage V with the same frequency as the travelling wave. The alternating current produced by this voltage in the circuit must also travel through the discharge. The current cannot be transferred directly by the travelling wave itself. The displacement of the space charge that produces the accompanying field $E(x,t)$ results in a current of no more than 1/1000 of the observed current at most. For this reason the alternating current, like the direct current, must be transferred without spatial variations by electrons in the plasma: the column must therefore contain a purely time-dependent oscillation as well as the travelling wave. (As we shall see, this also provides the explanation for the sinusoidal spatial modulation of the wave amplitude shown in fig. 5.) The system thus contains a travelling wave that owes its continued existence to a self-maintaining oscillation. Explaining how the striations in the plasma are linked with the current in the circuit thus amounts to explaining the coupling between the travelling wave and the oscillation in the plasma. In the following section it will be shown that a description of the phenomena in the plasma that takes both the travelling wave and the oscillation into account can provide a satisfactory explanation, leading to results that agree with the observations discussed, including the laser-type resonances.

Mathematical description

The local variations ($u(x,t)$) in the radiation from the discharge that are due to striations can be described in terms of a travelling wave:

$$u(x,t) = \mathrm{e}^{ax}\cos(\omega t - kx), \qquad (2)$$

where x is the distance from the cathode, a the rate of increase of the amplitude, ω the angular frequency and k the wave number of the travelling wave. The sinusoidal modulation of the amplitude is not taken into account. It is also assumed that the feedback is too weak for saturation of the amplitude at the anode.

The oscillation also affects the intensity. The effect of the travelling wave and the oscillation on the intensity of the radiation field can be described by the following equation:

$$u(x,t) = \mathrm{e}^{ax}\cos(\omega t - kx) + u_\mathrm{r}\cos(\omega t - \phi), \qquad (3)$$

where u_r is the relative amplitude of the oscillation and ϕ the phase difference between the travelling wave and the oscillation at the position $x = 0$. It is easy to see that the amplitude A of the resulting wave is given by

$$A(x) = \sqrt{\mathrm{e}^{2ax} + 2u_\mathrm{r}\mathrm{e}^{ax}\cos(kx - \phi) + u_\mathrm{r}^2}. \qquad (4)$$

This expression reproduces exactly what we have seen in fig. 5: a sinusoidal spatial modulation of an exponentially increasing signal. This gives an indication that the oscillation does indeed occur not only in the circuit but also in the discharge.

In fig. 5 we found a particular point where the change in intensity is always zero, irrespective of the value of the resistance included in the circuit. At position $x = x_0$ destructive interference occurs. This implies that the travelling wave and the oscillation at $x = x_0$ have the same intensity and also that their phase difference is exactly 180°. This point fits into this description as a boundary condition: $kx_0 = \pi + \phi$, and $u_\mathrm{r} = \mathrm{e}^{ax_0}$, which determines the coupling between the oscillation and the travelling wave.

The frequency spectrum

The resonances that occur in the current in the circuit and in the intensity of the photodiode signal can be explained in terms of the description of the wave phenomena in the discharge. As noted earlier, both

the optical intensity in the discharge and also the electric field accompanying the travelling wave satisfy an equation like equation (2). We were able to treat the plasma as an alternating voltage source supplying a voltage $V(t)$ (see page 94). Equation (1) shows that the alternating voltage between the cathode and anode is the integral of this field between $x = 0$ and $x = l$. This alternating voltage and the current it produces in the circuit must also satisfy Ohm's law:

$$V(t) = I(t)\,(Z + R), \qquad (5)$$

where Z is the impedance [4] of the plasma. Between the source voltage $V(t)$ (associated with the travelling wave) and the alternating current $I(t)$ in the circuit (associated with the oscillation) there must therefore be a fixed phase difference, because of Ohm's law. On integrating equation (1) it can be seen that this phase difference is directly connected with the terms in which sin kl and cos kl occur. Since the length of the tube is fixed, this phase difference can only agree with Ohm's law for particular values of k. If k_0 is a possible value at which Ohm's law is satisfied, then all other possible values are related to it by $kl = k_0 l + m2\pi$, where m is an integer. As the relation between the frequency and the wave number of the travelling wave is set by the dispersion relation (a characteristic property of the plasma), it follows that the frequency of the wave and hence the frequency of the oscillation can only assume specific values. This explains the resonances shown in figs 6 and 7 in the intensity of the radiation and in the current in the circuit.

[4] With Pekarek's model as the starting point an expression has been derived for the impedance Z in: F. C. van den Heuvel and Q. H. F. Vrehen, Striations of the convective type and feedback in low-pressure mercury/noble-gas discharges, Phys. Fluids **28**, 3034-3039, 1985.

The argument given above demonstrates that an oscillation occurs in the discharge and in the circuit. It is now clear that a study of the discharge alone is not sufficient for a proper understanding of the striation effects in the discharge. It has been shown that Pekarek's model, which only describes the processes in the discharge, can be extended to take the effect of the electrical circuit into account. Results obtained with this model are in quantitative agreement with observations. In a convective plasma striations can be suppressed by including in the circuit a filter that gives a high attenuation at frequencies within the 'gain bandwidth' for striations. The more fundamental origin of the coupling between the travelling wave in the discharge and the current it produces in the circuit requires further investigation, however. Our measurements demonstrate that a better understanding of this coupling can be obtained by studying the point at the start of the positive column where the total intensity variation is always zero.

Summary. In a gas discharge optical instabilities, called striations, can occur in certain circumstances. In a convectively unstable plasma a study has been made of the relation between these instabilities and the electrical circuit including the discharge. Feedback via the circuit produces an alternating current that has the effect of maintaining the striations in the plasma. A better understanding of the striations can be obtained by treating the plasma and the electrical circuit as a single entity. Measurements reveal an interesting boundary condition, requiring further investigation, for the interaction between the effects in the plasma and the alternating current in the circuit. The origin of this boundary condition must lie in the discharge itself.

Philips Tech. Rev. 44, No. 3, 96-100, July 1988

Scientific publications

These publications are contributed by staff from the laboratories and other establishments that form part of or are associated with the Philips group of companies. Many of the articles originate from the research laboratories named below. The publications are listed alphabetically by journal title.

Laboratory	Code
Philips GmbH Forschungslaboratorium Aachen, Weißhausstraße, 5100 Aachen, Germany	*A*
Philips Research Laboratory, Brussels, 2 avenue Van Becelaere, 1170 Brussels, Belgium	*B*
Philips Natuurkundig Laboratorium, Postbus 80 000, 5600 JA Eindhoven, The Netherlands	*E*
Philips GmbH Forschungslaboratorium Hamburg, Vogt-Kölln-Straße 30, 2000 Hamburg 54, Germany	*H*
Laboratoires d'Electronique et de Physique Appliquée, 3 avenue Descartes, 94450 Limeil-Brévannes, France	*L*
Philips Laboratories, N.A.P.C., 345 Scarborough Road, Briarcliff Manor, N.Y. 10510, U.S.A.	*N*
Philips Research Laboratories, Cross Oak Lane, Redhill, Surrey RH1 5HA, England	*R*
Philips Research Laboratories, Sunnyvale, P.O. Box 9052, Sunnyvale, CA 94086, U.S.A.	*S*

Authors	Lab	Title	Journal	Pages	Year
A. J. den Boef	*E*	Interferometric laser rangefinder using a frequency modulated diode laser	Appl. Opt. **26**	4545-4550	1987
D. J. Gravesteijn, H. M. van Tongeren*, M. Sens*, T. Bertens* (**Philips & Dupont Opt. Company, Eindhoven*) & C. J. van der Poel	*E*	Phase-change optical data storage in GaSb	*ibid.*	4772-4776	1987
J. C. M. Henning & J. P. M. Ansems	*E*	Determination of the photoionization threshold of the deep donor in $Al_{0.33}Ga_{0.67}As$:Si	Appl. Phys. A **44**	245-247	1987
D. J. Olego, J. Petruzzello, S. K. Ghandi*, N. R. Taskar* & I. B. Bhat* (**Rensselaer Polytech. Inst., Troy, NY*)	*N*	Elastic strains in CdTe-GaAs heterostructures grown by metalorganic chemical vapor deposition	Appl. Phys. Lett. **51**	127-129	1987
C. van Berkel & M. J. Powell	*R*	Resolution of amorphous silicon thin-film transistor instability mechanisms using ambipolar transistors	*ibid.*	1094-1096	1987
M. J. Powell, C. van Berkel, I. D. French & D. H. Nicholls	*R*	Bias dependence of instability mechanisms in amorphous silicon thin-films transistors	*ibid.*	1242-1244	1987
D. J. Olego	*N*	Effects of ZnSe epitaxial growth on the surface properties of GaAs	*ibid.*	1422-1424	1987
M. Nikoonahad	*N*	Differential amplitude contrast in acoustic microscopy	*ibid.*	1687-1689	1987
J. Khurgin	*N*	Second-order susceptibility of asymmetric coupled quantum well structures	*ibid.*	2100-2102	1987
P. Boher, M. Renaud, J. M. Lopez-Villegas, J. Schneider & J. P. Chane	*L*	InGaAs/Si_3N_4 interface obtained in ultrahigh vacuum multipolar plasma: *in-situ* control by ellipsometry and electrical characterization	Appl. Surf. Sci. **30**	100-107	1987
A. H. van Ommen	*E*	Diffusion of group III and V elements in SiO_2	*ibid.*	244-264	1987
A. H. van Ommen & M. P. A. Viegers	*E*	Buried oxide formation in Si high-dose implantation of oxygen	*ibid.*	383-389	1987
F. F. Leopold* & F. L. van Nes* (**Inst. Perception Res., Eindhoven*)		Control of data processing systems by voice commands	Behav. & Inf. Technol. **6**	323-326	1987
M. Wolny, T. Aguila, P. Deconinck, D. Moroni & J. P. André	*L*	High-performance WN-gate MISFETs fabricated from MOVPE wafers	Electron. Lett. **23**	1127-1128	1987
C. J. Mahon & G. D. Khoe	*E*	Endless polarisation state matching control experiment using two controllers of finite control range	*ibid.*	1234-1235	1987

Authors	Title	Journal	Pages	Year
F. Roozeboom, A. Sikkema & L. W. Molenkamp *E*	Multiple quantum well structures and high-power lasers of GaAs-AlGaAs grown by metalorganic vapor phase epitaxy (MOVPE)	Fiber & Integrated Opt. **6**	331-345	1987
P. R. Boudewijn & K. T. F. Janssen *E*	Application of SIMS in semiconductor research	Frensenius Z. Anal. Chem. **329**	215-219	1987
E. K. Broadbent, M. Delfino, A. E. Morgan, D. K. Sadana & P. Maillot *S*	Self-aligned silicided (PtSi and $CoSi_2$) ultra-shallow p^+/n junctions	IEEE **EDL-8**	318-320	1987
S. Colak, R. Eppenga & M. F. H. Schuurmans *E,N*	Band mixing effects on quantum well gain	IEEE J. **QE-23**	960-968	1987
W. C. H. Gubbels, C. D. Hartgring, R. H. W. Salters, J. A. M. Lammerts, M. J. Tooher, P. F. P. C. Hens, J. J. J. Bastiaens, J. M. F. van Dijk & M. A. Sprokel *E*	A 40-ns/100-pF low-power full-CMOS 256K (32KX8) SRAM	IEEE J. **SC-22**	741-747	1987
E. Seevinck, F. J. List & J. Lohstroh *E*	Static-noise margin analysis of MOS SRAM cells	*ibid.*	748-754	1987
A. J. E. M. Janssen *E*	A note on 'Positive time-frequency distributions'	IEEE Trans. **ASSP-35**	701-703	1987
P. C. W. Sommen, P. J. van Gerwen, H. J. Kotmans & A. J. E. M. Janssen *E*	Convergence analysis of a frequency-domain adaptive filter with exponential power averaging and generalized window function	IEEE Trans. **CAS-34**	788-798	1987
A. Bhattacharyya, S. N. Shabde, F. Barman & R. S. Muller (*Univ. of California, Berkeley, CA*) *S*	The effects of constant-current stress on gate oxides in LDD MOSFET's	IEEE Trans. **ED-34**	942-944	1987
S. J. Battersby & J. J. Harris *R*	Millimeter-wave bulk unipolar mixer diodes	*ibid.*	1046-1051	1987
G. A. M. Hurkx *E*	On the sidewall effects in submicrometer bipolar transistors	*ibid.*	1939-1946	1987
A. A. Staals*, M. C. van Houwelingen*, H. F. Huisman* (**PD Magnetics, Oosterhout*) & C. A. M. Mulder *E*	Localization and characterization of sub-surface particles in magnetic tape	IEEE Trans. **MAG-23**	112-114	1987
J. J. M. Ruigrok & D. Quak (*Univ. of Technol., Delft*) *E*	An alternative expression for the read flux in magnetic recording theory	*ibid.*	1764-1766	1987
B. J. Minnis *R*	Decade bandwidth bias T's for MIC applications up to 50 GHz	IEEE Trans. **MTT-35**	597-600	1987
W. J. A. M. Hartmann & H. M. J. Hikspoors (*Philips Consumer Electron. Div., Eindhoven*) *E*	Three-dimensional TV with cordless FLC spectacles	Inf. Disp. **3** (No. 9)	15-17	1987
A. F. de Jong, W. Coene* & H. Bender* (**Univ. Antwerpen*) *E*	HRTEM study of GaAs/AlAs interfaces: comparison of experimental, calculated and processed images	Inst. Phys. Conf. Ser. No. 87	9-14	1987
A. H. van Ommen & M. P. A. Viegers *E*	Structural study of the formation of a buried oxide layer by oxygen implantation	*ibid.*	385-390	1987
A. H. Reader, I. J. Raaijmakers & H. J. van Houtum *E*	Stacking faults and precipitates in annealed and co-sputtered C49 $TiSi_2$ films	*ibid.*	523-528	1987
C. W. T. Bulle-Lieuwma, A. H. van Ommen & J. Hornstra *E*	Structural study of $CoSi_2$ grown on (001) and (111) Si	*ibid.*	541-546	1987
W. J. Bartels *E*	Computer simulation of X-ray diffraction profiles for the characterization of superlattices	*ibid.*	599-608	1987
S. M. Smith*, N. J. Cronin*, (**Univ. of Bath*), R. J. Nicholas⁺, M. A. Brummell⁺ (⁺*Clarendon Lab., Oxford*) & J. J. Harris & C. T. Foxon *R*	Millimeter and submillimeter detection using $Ga_{1-x}Al_xAs$/GaAs heterostructures	Int. J. Infrared & Millimeter Waves **8**	793-802	1987
Y. Genin *B*	A survey of the eigenstructure properties of finite Hermitian Toeplitz matrices	Integral Equations & Operator Theory **10**	621-639	1987

Authors	Title	Journal	Pages	Year
W. M. Rabinowitz*, A. J. M. Houtsma (*Inst. for Perception Res., Eindhoven*), N. I. Durlach* & L. A. Delhorne* (**Massachusetts Inst. of Technol., Cambridge, MA*)	Multidimensional tactile displays: identification of vibratory intensity, frequency, and contactor area	J. Acoust. Soc. Am. **82**	1243-1252	1987
S. G. Nooteboom (*Inst. for Perception Res., Eindhoven & Univ. Leiden*) & J. G. Kruyt (*Inst. for Dutch Lexicol., Leiden*)	Accents, focus distribution, and the perceived distribution of given and new information: an experiment	*ibid.*	1512-1524	1987
J. H. M. van der Linden, P. E. Wierenga & E. P. Honig *E*	Viscoelastic behaviour of polymer layers with inclusions	J. Appl. Phys. **62**	1613-1615	1987
H. A. van Sprang & H. G. Koopman *E*	Temperature compensation of the threshold voltage of a 270° twist (SBE) cell	*ibid.*	1734-1738	1987
M. Delfino, A. E. Morgan, E. K. Broadbent, P. Maillot & D. K. Sadana *S*	Effect of post-silicidation annealing on $TiSi_2/p^+$-n Si junctions	*ibid.*	1882-1886	1987
P. A. Breddels, H. A. van Sprang & J. Bruinink *E*	Influence of dispersion on the transmission characteristics of supertwisted nematic effects in liquid-crystal displays	*ibid.*	1964-1967	1987
S. Colak, J. Khurgin, W. Seemungal & A. Hebling *N*	Threshold in electron-beam end-pumped II-VI lasers	*ibid.*	2633-2639	1987
D. K. Sadana, A. E. Morgan, M. H. Norcott & Naik *S*	Annealing and oxidation behavior of low-pressure chemical vapor deposited tungsten slicide layers on polycrystalline silicon gates	*ibid.*	2830-2835	1987
D. A. Cammack, R. J. Dalby, H. J. Cornelissen & J. Khurgin *N*	Electron beam pumped lasing in ZnSe/ZnSSe superlattice structures grown by molecular-beam epitaxy	*ibid.*	3071-3074	1987
R. Pandya & B. A. Khan *N*	Transient photocurrent response in polycrystalline silicon thin films	*ibid.*	3244-3248	1987
P. H. Oosting, J. Petruzzello & T. F. McGee *E,N*	Formation of buried nitride silicon-on-insulator structures studied by Auger electron spectroscopy and transmission electron microscopy	*ibid.*	4118-4123	1987
H. Mani*, A. Joullie*, J. Bhan* (**EM-CNRS, Montepellier*), C. Schiller & J. Primot (*CNET, Bagneux*) *L*	The influence of supercooling on the liquid phase epitaxial growth of $InAs_{1-x}Sb_x$ on (100) GaSb substrates	J. Electron. Mater. **16**	289-294	1987
F. R. de Boer*, Huang Ying-Kai* (**Univ. Amsterdam*), D. B. de Mooij & K. H. J. Buschow *E*	Magnetic properties of a series of novel ternary intermetallics ($RFe_{10}V_2$)	J. Less-Common Met. **135**	199-204	1987
D. B. de Mooij & K. H. J. Buschow *E*	Some novel ternary $ThMn_{12}$-type compounds	J. Less-Common Met. **136**	207-215	1988
R. Grössinger*, H. Kirchmayr* (**Univ. of Technol., Vienna*) & K. H. J. Buschow *E*	Magnetic anisotropy in the system $La_2Fe_{14-x}Co_xB$ and its relation to the system $Nd_2Fe_{14-x}Co_xB$	*ibid.*	367-373	1988
P. Schobinger-Papamantellos (*Inst. für Kristallogr. und Petrogr., Zürich*) & K. H. J. Buschow *E*	Magnetic structure changes observed by neutron diffraction in the system $TbGe_{1-x}Si_x$ ($0.4 \leq x \leq 1.0$)	J. Magn. & Magn. Mater. **71**	134-146	1988
C. A. M. Mulder & A. A. J. M. Damen *E*	The origin of the 'defect' 490 cm^{-1} Raman peak in silica gel	J. Non-Cryst. Solids **93**	387-394	1987
G. A. C. M. Spierings *E*	Optical absorption of Ag^+ ions in $11(Na, Ag)_2O \cdot 11B_2O_3 \cdot 78SiO_2$ glass	J. Non-Cryst. Solids **94**	407-411	1987
C. A. M. Mulder *E*	Defect structures in silica glass	J. Non-Cryst. Solids **95 & 96**	303-310	1987
J. W. C. de Vries *E*	Surface scattering in thin evaporated gold double layers studied by *in situ* resistivity measurements	J. Phys. F **17**	2403-2409	1987
P. Schobinger-Papamantellos (*Inst. für Kristallogr. und Petrogr., Zürich*) & K. H. J. Buschow *E*	The magnetic phase diagram of $HoGe_{1-x}Si_x$ studied by neutron diffraction and magnetic measurements	J. Solid State Chem. **70**	249-261	1987
P. Friedel, J.-P. Landesman, P. Boher & J. Schneider *L*	Cleaning and nitridation of GaAs surfaces in multipolar plasmas investigated by *in situ* photoemission and spectroscopic ellipsometry	J. Vac. Sci. & Technol. **B 5**	1129-1134	1987

J. van Zwol, J. van Laar, A. W. Kolfschoten & J. Dieleman *E*	Effects of Ar^+ angle of incidence on the etching of Si with Cl_2 and low-energy Ar^+ ions	J. Vac. Sci. & Technol. B **5**	1410-1414	1987
W. C. M. Claassen & J. Dieleman *E*	An *in situ* infrared study on the interaction of oxygen plasmas with Si and fluorine plasmas with SiO_2 surfaces	*ibid.*	1450-1452	1987
J. K. Annot & R. A. H. van Twist *E*	A novel deadlock free and starvation free packet switching communication processor	Lecture Notes in Computer Science, Vol. 258, G. Goos & J. Hartmanis (eds), Springer, Berlin	68-85	1987
E. A. M. Odijk *E*	The DOOM system and its applications: a survey of Esprit 415 subproject A, Philips Research Laboratories	*ibid.*	461-479	1987
L. Augusteijn *E*	Garbage collection in a distributed environment	Lecture Notes in Computer Science, Vol. 259, G. Goos & J. Hartmanis (eds), Springer, Berlin	75-93	1987
A. H. Reader, A. H. van Ommen & H. J. W. van Houtum *E*	Resistivity differences in C49 $TiSi_2$ films formed by rapid thermal processing	Mater. Res. Soc. Symp. Proc. **92**	177-182	1987
A. H. van Ommen, H. J. Ligthart, J. Politiek & M. P. A. Viegers *E*	High-quality SOI by oxygen implantation into silicon	Mater. Res. Soc. Symp. Proc. **93**	119-123	1987
E. Gerritsen, H. J. Ligthart & T. E. G. Daenen *E*	Cross-sectional TEM and corrosion studies of Al and N implanted copper	*ibid.*	329-334	1987
W. J. A. Goossens *E*	The smectic A and the smectic C phase: a coherent molecular picture	Mol. Cryst. & Liq. Cryst. **150b**	419-445	1987
D. J. Verschuur*, D. de Vries* (**Univ. of Technol., Delft*), A. J. M. Kaizer & W. F. Druijvesteijn *E*	Toepassing van de Wignerdistributie bij de analyse van luidsprekerresponsies in kamers	Ned. Akoest. Genootschap nr. 87	31-45	1987
R. A. Haring (*IBM T. J. Watson Res. Center, Yorktown Heights, NY*), H. E. Roosendaal (*North-Holland Phys. Publishing, Amsterdam*) & P. C. Zalm *E*	On the energy and angular distribution of sputtered polyatomic molecules	Nucl. Instrum. & Methods Phys. Res. **B28**	205-213	1987
J. P. Charlier, M. Vanbegin & P. van Dooren *B*	On efficient implementations of Kogbetliantz's algorithm for computing the singular value decomposition	Numer. Math. **52**	279-300	1988
J. W. M. Bergmans & A. J. E. M. Janssen *E*	Robust data equalization, fractional tap spacing and the Zak transform	Philips J. Res. **42**	351-398	1987
J. W. M. Bergmans, S. A. Rajput & F. A. M. van de Laar *E*	On the use of decision feedback for simplifying the Viterbi detector	*ibid.*	399-428	1987
P. P. J. van Engelen & K. H. J. Buschow *E*	The magneto-optical properties of Heusler alloys of the type $Co_{2-x}Cu_xMnSn$	*ibid.*	429-434	1987
P. K. Bachmann *E*	Worldwide status of dispersion-modified single-mode fibres	*ibid.*	435-450	1987
C. Ronse *B*	On rotators and shifters	*ibid.*	451-479	1987
R. Eppenga, M. F. H. Schuurmans & S. Colak *E*	New k·p theory for $GaAs/Ga_{1-x}Al_xAs$-type quantum wells	Phys. Rev. B. **36**	1554-1564	1987
D. B. M. Klaassen, C. M. G. van Leuken & K. M. H. Maessen (*Univ. Utrecht*) *E*	'Giant resonances' in luminescence soft-X-ray excitation spectra of phosphors	*ibid.*	4407-4412	1987
D. K. Maude*, J. C. Portal+, L. Dmowski+ (+*INSA, Toulouse & SNCI-CNRS, Grenoble*), T. Foster*, L. Eaves* (**Univ. Nottingham*), M. Nathan[0], M. Heiblum[0] ([0]*IBM, T. J. Watson Res. Center, Yorktown Heights, NY*), J. J. Harris & R. B. Beall *R*	Investigation of the DX center in heavily doped n-type GaAs	Phys. Rev. Lett. **59**	815-818	1987
R. N. Bhargava, S. P. Herko & W. N. Osborne *N*	Improved high-T_c superconductors	Phys. Rev. Lett. **59**	1468-1471	1987

H. M. J. Boots	*E*	Inhomogeneous network formation studied by the kinetic gelation model	Physica **147A**	90-98	1987
C. W. J. Beenakker	*E*	Two-dimensional soap froths and polycrystalline networks: why are large cells many-sided?	*ibid.*	256-267	1987
E. E. Havinga, L. W. van Horssen, W. ten Hoeve (*Syncom, Groningen*), H. Wynberg (*Univ. Groningen*) & E. W. Meijer	*E*	Self-doped water-soluble conducting polymers	Polym. Bull. **18**	277-281	1987
M. R. Haghiri	*L*	Delayed decision in motion compensation technique and its application to images coding	Proc. 2nd Int. Conf. on Image processing and its applications, London 1986	205-209	1986
H. Baudry	*L*	Screen printing piezoelectric devices	Proc. 6th Eur. Microelectronics Conf., Bornemouth 1987	71-74	1987
P. Martin, T. Bonnet & Y. Mathieu	*L*	Circuit systolique pour la synthese d'images	Proc. Colloq. MARI '87, Paris - La Villette 1987	112-117	1987
C. Blanc, P. Pesqué & O. Bonnefous	*L*	Comparison between various beam forming techniques for ultrasound imaging	Proc. Conf. Int. Ultrasonics '87, London 1987	333-338	1987
A. Fihel & H. Sari	*L*	Reduced-bandwidth QAM signaling for digital radio relay systems	Proc. Eur. Conf. on Radio-relay systems, Munich 1986	173-181	1986
M. R. Haghiri & B. Boutrois	*L*	Tree motion estimation algorithm for video sequence	Proc. IEEE Int. Conf. on Communications, Seattle, WA, 1987	141-146	1987
M. Lamnabhi & M. Louafi	*L*	Burst mode operation of phase-locked loops in the presence of noise	*ibid.*	207-212	1987
S. Moridi & H. Sari	*L*	Effect of loop delay on the pull-in range of generalized second-order phase locked loops	*ibid.*	1041-1045	1987
H. Sari & G. Karam	*L*	Cancellation of power amplifier nonlinearities in digital radio receivers	*ibid.*	1809-1814	1987
P. Dawson, K. J. Moore & C. T. Foxon	*R*	Photoluminescence studies of type II GaAs/AlAs quantum wells grown by MBE	Proc. SPIE **792**	208-213	1987
J. Braat	*E*	Quality of microlithographic projection lenses	Proc. SPIE **811**	22-30	1987
E. W. Meijer, M. C. Raas & P. N. T. van Velzen	*E*	A specific 2,4-disubstituted-adamantane interaction with plasma-grown aluminium oxide. An inelastic-electron-tunnelling spectroscopy study	Recl. Trav. Chim. Pays-Bas **106**	521-525	1987
J. J. van den Broek & A. G. Dirks	*E*	Metastable phases in binary alloy films	Scr. Metall. **21**	1469-1474	1987
J. C. Brice, P. Capper, B. C. Easton, J. L. Page & P. A. C. Whiffin	*R*	Growth and characterisation of $Cd_xHg_{1-x}Te$ grown by LPE using a novel sliding boat	Semicond. Sci. Technol. **2**	710-715	1987
F. J. J. Blommaert*, H. G. M. Heynen* & J. A. J. Roufs* (**Inst. Perception Res., Eindhoven*)		Point spread functions and detail detection	Spatial Vision **2**	99-115	1987
J. B. Clegg	*R*	Depth profiling of shallow arsenic implants in silicon using SIMS	Surf. & Interface Anal. **10**	332-337	1987
P. C. Zalm	*E*	Quantitative sputtering	Surf. & Interface Anal. **11**	1-24	1988
J. Aarts & P. K. Larsen	*E*	Monolayer and bilayer growth on Ge(111) and Si(111)	Surf. Sci. **188**	391-401	1987
P. J. van Otterloo	*E*	A contour-oriented approach to digital shape analysis	Thesis, Delft	1-369	1988
P. J. M. van Laarhoven	*E*	Theoretical and computational aspects of simulated annealing	Thesis, Rotterdam	1-173	1988
A. G. Tangena & P. J. M. Wijnhoven	*E*	The correlation between mechanical stresses and wear in a layered system	Wear **121**	27-35	1988

Volume 44, No. 3 pages 61-100 Published 14th July 1988

PHILIPS

J. J. Kelly, J. E. A. M. van den Meerakker, P. H. L. Notten and R. P. Tijburg, Wet-chemical etching of III-V semiconductors,

Philips Tech. Rev. 44, No. 3, 61-74, July 1988.

III-V semiconductors like GaAs can be wet-chemically etched by three mechanisms: electrochemically with an external voltage source, electrochemically using an oxidizing agent (electroless), and chemically with a reactive compound. In some cases the etching process only proceeds when the semiconductor is exposed to light. The etch rate depends on the relative reaction rate at the semiconductor surface and the mass transfer in the solution. Other important factors are the effect of the crystal planes, the orientation of a mask with respect to these planes, and the electrical contact with other materials. Wet-chemical etching of III-V semiconductors can be used on a large scale for various applications, including the detection of crystallographic defects, the fabrication of special profiles and the selective dissolution of closely related materials in multilayer structures.

J. J. Ponjeé and P. N. T. van Velzen, Chemical modification of surfaces,

Philips Tech. Rev. 44, No. 3, 81-88, July 1988.

Bifunctional organic molecules that form bonds with a surface with one functional group give new properties to the surface with the other functional group. Adhesion to a surface or release from a surface can be improved by using this method. Preconditions for such chemical surface modification are the presence of reactive sites at the surface, the absence (because of good cleaning procedures) of impurities at these sites, and the possibility of stress relaxation on expansion and shrinkage. Subjects discussed include improvement of the adhesion between a photosensitive resist based on 'novolac' and silicon with an aminosilane, improved adhesion between noble metals and glass with a mercaptosilane, improved adhesion of silver reflecting coatings on LaserVision discs with tannin, an improvement of both adhesion and release in the replication method used for making aspheric lenses, using a methacryloxysilane and a trialkylsilane. The chemical surface modifications described here for the replication method have been investigated by IETS and TOF-SIMS. The principles of these methods are discussed and some results are presented.

A. I. Kucharska, P. Blood and E. D. Fletcher, Bistability in quantum-well lasers,

Philips Tech. Rev. 44, No. 3, 76-80, July 1988.

Hysteresis has been observed in the light-current characteristics of inhomogeneously pumped GaAs-$Al_xGa_{1-x}As$ laser structures which were grown by molecular beam epitaxy and whose active regions consisted of 2.5 nm thick multiple quantum wells (MQW). Fast switching ($<$ 2 ns) between low and high light-output levels was demonstrated. The observed bistability was due to saturation of the optical absorption in the passive region of these structures at high injection currents. The MQW laser devices operated in the wavelength region of the excitonic absorption and their bistability was ascribed to the decrease of this absorption at higher light intensities.

F. C. van den Heuvel, Striations in a gas discharge,

Philips Tech. Rev. 44, No. 3, 89-95, July 1988.

In a gas discharge optical instabilities, called striations, can occur in certain circumstances. In a convectively unstable plasma a study has been made of the relation between these instabilities and the electrical circuit including the discharge. Feedback via the circuit produces an alternating current that has the effect of maintaining the striations in the plasma. A better understanding of the striations can be obtained by treating the plasma and the electrical circuit as a single entity. Measurements reveal an interesting boundary condition, requiring further investigation, for the interaction between the effects in the plasma and the alternating current in the circuit. The origin of this boundary condition must lie in the discharge itself.

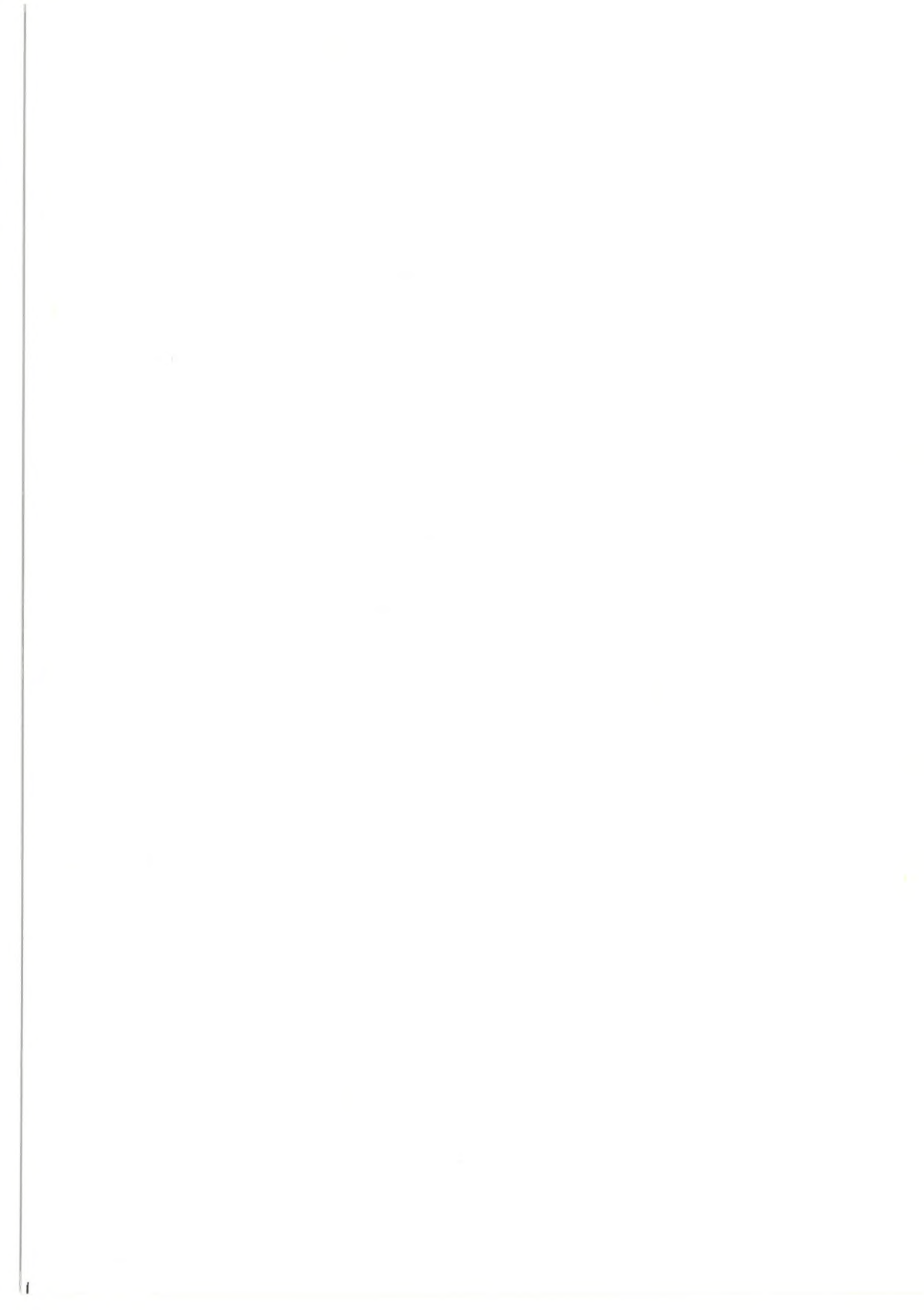

OTHER PHILIPS PUBLICATIONS

Philips Journal of Research

An English-language journal with articles on research at the various Philips Laboratories. Six issues per volume.
Information: Philips Journal of Research, Philips Research Laboratories, P.O. Box 80 000, 5600 JA Eindhoven.

Acta Electronica

An annual publication with a special subject for each year, with articles in French and English on electronics and applied physics.
Information: Acta Electronica, Laboratoires d'Electronique et de Physique appliquée, 3 Avenue Descartes, 94451 Limeil-Brévannes Cedex, France.

Philips Telecommunication and Data Systems Review

An English-language journal, dealing with developments, systems, and products in business communications, computers, computer networks, telecommunications services, radio communications and dictation equipment. Four issues per volume.
Information: Philips Telecommunication and Data Systems Review, P.O. Box 32, 1200 JD Hilversum, The Netherlands.

Electronic Components and Applications

An English-language journal with articles dealing with electronic components and materials and their applications. Four issues per volume.
Information: Electronic Components and Applications, Philips Electronic Components and Materials Division, P.O. Box 218, 5600 MD Eindhoven, The Netherlands.

Medicamundi

An English-language journal with articles on radiology, isotope diagnosis and medical electronics. Three issues per volume.
Information: Medicamundi, Philips Nederland, Boschdijk 525, 5621 JG Eindhoven, The Netherlands.

Forthcoming issues of Philips Technical Review will include articles on:

- Polyepoxides
- Magnetic domains in amorphous alloys
- Noise suppression in electrical appliances
- Magnetic-recording heads

Philips Tech. Rev. Vol. 44, No. 3, July 1988

Contents

Page

Wet-chemical etching of III-V semiconductors . . . . . J. J. Kelly, . . . J. E. A. M. van den Meerakker, P. H. L. Notten and R. P. Tijburg 61

Then and now (1938-1988) 75

Bistability in quantum-well lasers . . . . A. I. Kucharska, P. Blood and E. D. Fletcher 76

Chemical modification in surfaces . . . . J. J. Ponjeé and P. N. T. van Velzen 81

Striations in a gas discharge . . . . F. C. van den Heuvel 89

Scientific publications 96

PHILIPS TECHNICAL REVIEW
Philips Research Laboratories
P.O. Box 80 000
5600 JA Eindhoven
The Netherlands

Subscription rate per volume	fl. 80.00 or U.S. $ 35.00
Student's subscription	fl. 32.00 or U.S. $ 14.00
Binder	fl. 10.00 or U.S. $ 4.00

Payment only after invoicing, please.

Printed in the Netherlands

PHILIPS